JOURNAL OF GEOPHYSICAL RESEARCH, VOL. 112, C05017, doi:10.1029/2006JC003731, 2007

A modeling study of the seasonal oxygen budget of the global ocean

X. Jin,[1] R. G. Najjar,[2] F. Louanchi,[3] and Scott C. Doney[4]

Received 25 May 2006; revised 20 October 2006; accepted 14 November 2006; published 9 May 2007.

[1] An ecosystem model embedded in a global ocean general circulation model is used to quantify roles of biological and physical processes on seasonal oxygen variations. We find that the thermally induced seasonal net outgassing (SNO) of oxygen is overestimated by about 30% if gas phase equilibrium is assumed, and we find that seasonal variations in thermocline oxygen due to biology are approximated well using the oxygen anomaly. Outside the tropics and the north Indian Ocean, biological SNO is, on average, 56% of net community production (defined as net oxygen production above 76 m) during the outgassing period and 35% of annual net community production. In the same region the seasonal drawdown of the oxygen anomaly within the upper thermocline (76–500 m) is 76% of the remineralization during the drawdown and 48% of annual remineralization. Applying model-derived relationships to observed O_2 climatologies and using independent estimates for tropical and monsoonal systems, we estimate global net community production to be 14.9 ± 2.5 Pg C yr^{-1}.

Citation: Jin, X., R. G. Najjar, F. Louanchi, and S. C. Doney (2007), A modeling study of the seasonal oxygen budget of the global ocean, *J. Geophys. Res.*, *112*, C05017, doi:10.1029/2006JC003731.

1. Introduction

[2] Reliable estimates of the net production of organic matter in surface waters, often referred to as net community production, export production or new production [e.g., *Eppley and Peterson*, 1979], are essential for a firm understanding of the global carbon cycle. One of the more robust methods of estimating net community production exploits the annual cycle of the air-sea oxygen flux [*Keeling and Shertz*, 1992; *Bender et al.*, 1996; *Najjar and Keeling*, 2000] and is based on the geochemical techniques pioneered by *Shulenberger and Reid* [1981], *Jenkins and Goldman* [1985], and *Emerson* [1987]. The method is appealing because atmospheric oxygen measurements integrate the air-sea oxygen flux over large areas, potentially reflecting net community production over a hemispheric scale. A difficulty, however, is that physical processes can confound the relationship between net community production and outgassing. For example, some O_2 produced during net community production is mixed downward and not immediately outgassed. Further, the annual cycle in the air-sea oxygen flux has contributions from processes other than production during the outgassing period, such as wintertime ventilation of oxygen-depleted waters in the seasonal thermocline and spatial and temporal variability in solubility. Similar problems arise when the annual cycle in oxygen is exploited to estimate shallow remineralization, another important yet difficult to estimate component of the global carbon cycle. The seasonal drawdown in O_2 in the seasonal thermocline [*Jenkins and Goldman*, 1985; *Najjar and Keeling*, 1997, 2000] may not be equal to respiration because of O_2 sources and sinks due to advection and diffusion and lateral fluxes of organic matter.

[3] Two recent studies have shed light on the factors affecting the annual cycle in the air-sea oxygen flux. *Nevison et al.* [2005] developed a technique for separating ventilation and production effects in the Southern Hemisphere using the annual cycle in atmospheric N_2O, which is driven, in part, by ventilation of N_2O-enriched waters in the seasonal thermocline. *Dietze and Oschlies* [2005] investigated a common approximation of the thermally induced oxygen flux (introduced by *Keeling et al.* [1993]) using a numerical model and found that the annual cycle is overestimated by about 20% due to the impact of penetrating solar radiation and surface mixing. We know of no studies that address the impact of physical processes on the seasonal drawdown of oxygen in the thermocline.

[4] The goal of this study is to quantify the relationship between marine biological rates of carbon cycling in the upper ocean (net community production and shallow remineralization) and the annual cycle of oxygen. We use a three-dimensional model of dissolved oxygen dynamics in the ocean for this purpose. The model consists of three components: the circulation model, a standard nitrogen-based ecosystem model, and an oxygen component. Our goal is not to achieve a perfect simulation of nitrogen and O_2 dynamics in the ocean but rather to establish relationships between the seasonality of oxygen and the carbon cycle rates of interest. We then apply these relationships to

[1]Institute of Geophysics and Planetary Physics and Department of Atmospheric and Oceanic Sciences, University of California, Los Angeles, California, USA.
[2]Department of Meteorology, Pennsylvania State University, University Park, Pennsylvania, USA.
[3]Institut des Sciences de la Mer et de l'Aménagement du Littoral, Algiers, Algeria.
[4]Department of Marine Chemistry and Geochemistry, Woods Hole Oceanographic Institution, Woods Hole, Massachusetts, USA.

0148-0227/07/2006JC003731$09.00

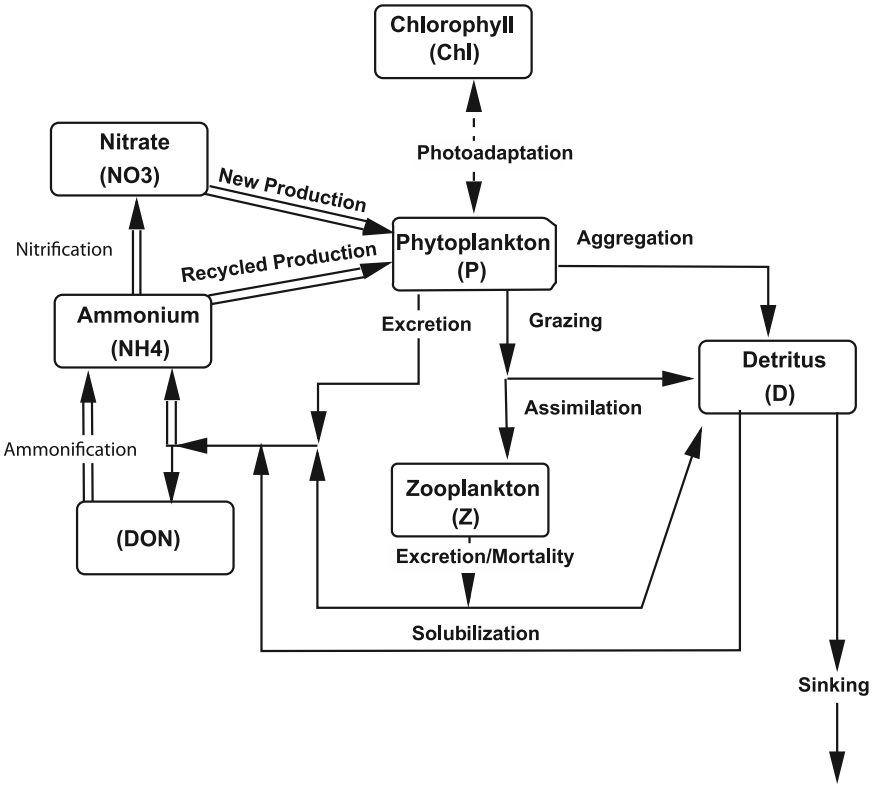

Figure 1. Schematic diagram of ecosystem model. Double lines show pathways during which oxygen is produced or consumed.

the observed ocean O_2 annual cycle to derive rates of net community production and shallow remineralization over large scales in the ocean.

2. Model Description

2.1. Physical Model

[5] The physical model used in this study is NCOM (NCAR CCSM Ocean Model), a coarse-resolution global general circulation model, which is a component of the Community Climate System Model (CCSM) developed at the National Center for Atmospheric Research (NCAR) [*Blackmon et al.*, 2001]. NCOM is based on the Geophysical Fluid Dynamics Laboratory (GFDL) Modular Ocean Model (MOM), version 1.1 [*Bryan*, 1969; *Cox*, 1984; *Pacanowski et al.*, 1991]. The model is described in detail by *Large et al.* [1997]; here we give a brief description. The model has a total of 25 levels in the vertical, with the uppermost level 12 m thick and 7 levels in the upper 200 m. The horizontal resolution is $1.8°-3.4°$ in latitude (with increased resolution at the equator and higher latitudes) and $3.6°$ in longitude. The main improvements to MOM are (1) the inclusion of the upper ocean vertical mixing model of *Large et al.* [1994], which leads to a more realistic exchange of properties between the surface layer and underlying seasonal thermocline [*Doney et al.*, 1996]; (2) surface bulk heat, freshwater and momentum forcing [*NCAR Oceanography Section*, 1996; *Doney et al.*, 1998], which produces improved annual cycles of sea surface temperature (SST) and mixed layer depth as well as better solutions for intermediate and deep water masses [*Large et al.*, 1997]; and (3) the isopycnal transport parameterization of *Gent and McWilliams* [1990], which diminishes the spurious upwelling and diapycnal diffusion of properties across western boundary currents [*Sarmiento et al.*, 1993; *Böning et al.*, 1995] and the Antarctic Circumpolar Current, a feature typically found in z coordinate models.

[6] The atmospheric data sets required by the bulk surface forcing scheme are generated from the National Center for Environmental Prediction (NCEP) reanalysis and cover the four years 1985 through 1988. The monthly mean fields include the zonal and meridional wind velocity components, air temperature, specific humidity, fractional cloud cover, and net downward short-wave radiation. Monthly mean sea surface temperature and salinity are from the climatologies of *Shea et al.* [1990] and *Levitus* [1982]. The forcing field values at each model time step are computed using linear interpolation. Details of the forcing scheme are given by *NCAR Oceanography Section* [1996] and *Large et al.* [1997].

2.2. Ecosystem Model

[7] The ecosystem model used in this study is based on the five-compartment, nitrogen-based model of *Doney et al.* [1996]. The model has been tested extensively for the Bermuda Atlantic Time series Study site in the Sargasso Sea and has been shown to replicate the basic features of the annual cycle, including the initiation of the winter-spring bloom and the summer deep chlorophyll maximum, two processes essential for simulation of the annual oxygen cycle. Because of the importance of dissolved organic matter to the marine carbon and oxygen cycles [*Hansell*

Table 1. List of Many of the Symbols Used in This Paper

Symbol	Definition	Units
A	surface area of a region	m^2
Chl	chlorophyll concentration	mg m^{-3}
C_p	specific heat of seawater	J kg^{-1} K^{-1}
D	detrital N concentration	mmol m^{-3}
DON	dissolved organic nitrogen concentration	mmol m^{-3}
f	sea ice fraction	
F_{O2}	net upward flux of O_2 at the air-sea interface	mmol m^{-2} s^{-1}
F_T^{Heat}	net upward flux of O_2 at the air-sea interface computed using equation (6)	mmol m^{-3}
F_T^{Model}	net upward flux of solubility O_2 at the air-sea interface in the numerical model	mmol m^{-2} s^{-1}
F_h	mean horizontal flux of O_2 into a region	mmol m^{-2} s^{-1}
F_{trans}	mean horizontal plus vertical flux of O_2 into a region	mmol m^{-2} s^{-1}
F_v^{bot}	mean flux of O_2 into a region across its bottom	mmol m^{-2} s^{-1}
F_v^{top}	mean flux of O_2 into a region across its top	mmol m^{-2} s^{-1}
k_w	O_2 gas transfer velocity	cm hr^{-1}
NCP	net community production	mol O_2
NH_4	ammonium concentration	mmol m^{-3}
Ni	nitrification rate	mmol N m^{-3} s^{-1}
NO_3	nitrate concentration	mmol m^{-3}
NP	new production	mmol N m^{-3} s^{-1}
$[O_2^b]$	biological oxygen concentration	mmol m^{-3}
$[O_2^s]$	solubility oxygen concentration	mmol m^{-3}
$[O_2^{sat}]$	oxygen saturation concentration	mmol m^{-3}
$[O_2^t]$	total oxygen concentration	mmol m^{-3}
P	phytoplankton N concentration	mol m^{-3}
Q	net upward heat flux at air-sea interface	W m^{-2}
r_{Ni}	O_2:N molar ratio during nitrification	
r_{NP}	O_2:N molar ratio during new production	
r_{RP}	O_2:N molar ratio during recycled production	
RM	remineralization	mol O_2
RP	recycled production	mol N m^{-3} s^{-1}
Sc_{O2}	Schmidt number for O_2	
S	sources minus sinks of O_2 or N	mmol m^{-3} s^{-1}
SNO	seasonal net outgassing	mol O_2
t	time	s
T	temperature	K
TOD	thermocline oxygen decline	mol O_2
u	10-m wind speed	m s^{-1}
X	conversion of organic N to ammonium	mmol N m^{-3} s^{-1}
V	volume of a region	m^3
Z	zooplankton concentration	mmol N m^{-3}
ρ	density	kg m^{-3}

and Carlson, 1998], we add dissolved organic nitrogen to our model. We also add ammonium to the model in order to differentiate between new and regenerated production. The ecosystem model then consists of seven prognostic variables (Figure 1): nitrate (NO_3), ammonium (NH_4), phytoplankton (P), zooplankton (Z), dissolved organic nitrogen (DON), detritus (D), and chlorophyll (Chl). Table 1 defines these and other variables in the paper. A detailed description of the model is given in Appendix A.

2.3. Oxygen Model

[8] In order to model the impact of biological processes on the oxygen cycle, the oxygen source/sink term is linked to nitrogen transformations. There are four distinct pathways in the model where oxygen is produced or consumed (Figure 1): the conversion of nitrate to organic nitrogen (new production), the conversion of ammonium to organic nitrogen (recycled production), the conversion of organic nitrogen to ammonium (ammonification, excretion, mortality and solubilization), and the conversion of ammonium to nitrate (nitrification). The C, H, N and O stoichiometry of these transformations follows *Libes* [1992, pp. 130, 133] and is given, respectively, by

$$\begin{gathered} 106CO_2 + 122H_2O + 16HNO_3 \rightarrow (CH_2O)_{106}(NH_3)_{16} + 138O_2 \\ 106CO_2 + 106H_2O + 16NH_3 \rightarrow (CH_2O)_{106}(NH_3)_{16} + 106O_2 \\ (CH_2O)_{106}(NH_3)_{16} + 106O_2 \rightarrow 106CO_2 + 106H_2O + 16NH_3 \\ 16NH_3 + 32O_2 \rightarrow 16HNO_3 + 16H_2O \end{gathered} \tag{1}$$

[9] Thus the net source of oxygen in the model is given by

$$S(O_2) = r_{NP}NP + r_{RP}RP - r_{Ni}Ni - r_{RP}X, \tag{2}$$

Table 2. Specification of the Three Forms of Oxygen Used in the Model

Variable	Net Sea-to-Air Flux	Net in situ Source	Initial Condition
Total oxygen (O_2^t)	$k_w([O_2^t]_{sfc} - [O_2^{sat}])$	$S(O_2^b)$	$[O_2]$
Biological oxygen (O_2^b)	$k_w[O_2^b]_{sfc}$	$S(O_2^b)$	$[O_2] - [O_2^{sat}]$
Solubility oxygen (O_2^s)	$k_w([O_2^s]_{sfc} - [O_2^{sat}])$	0	$[O_2^{sat}]$

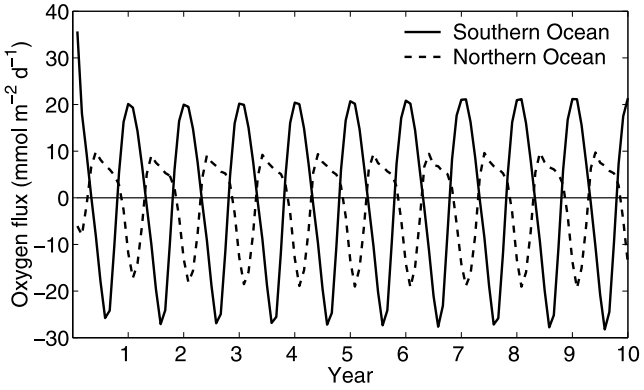

Figure 2. Model sea-to-air oxygen flux averaged over Northern and Southern Hemispheres as a function of time.

where the O_2:N ratios are r_{NP} = 138:16 during new production (NP), r_{RP} = 106:16 during recycled production (RP) and the transformation of organic nitrogen to ammonia (X), and r_{Ni} = 2:1 during nitrification (Ni). The traditional value of O_2:N during new production used here (138:16) is lower than more recent estimates, which range from 150:16 to 170:16 [*Anderson and Sarmiento*, 1994; *Anderson*, 1995]. There is no denitrification in the model, and thus the oxygen concentration is allowed to be less than zero.

[10] The sea-to-air flux of oxygen, F_{O_2}, is parameterized using a standard transfer velocity formulation:

$$F_{O_2} = k_w\left([\mathrm{O_2}] - \left[\mathrm{O_2^{sat}}\right]\right), \tag{3}$$

where k_w is the gas transfer velocity for oxygen, $[O_2]$ is the surface ocean oxygen concentration, and $[O_2^{sat}]$ is the oxygen saturation concentration. $[O_2]$ is predicted by the model and $[O_2^{sat}]$ is computed from the surface temperature (T) and salinity in the model using the formula of *Garcia and Gordon* [1992]. "Surface" values of tracers, such as $[O_2]$ in equation (3), actually reflect values for the uppermost layer of the model, which is 12 m thick. Bubble-induced supersaturation is not included because it is not well constrained over the spatial (basin-wide) and temporal (seasonal) timescales of interest here. Inert gas measurements at time series stations have accelerated

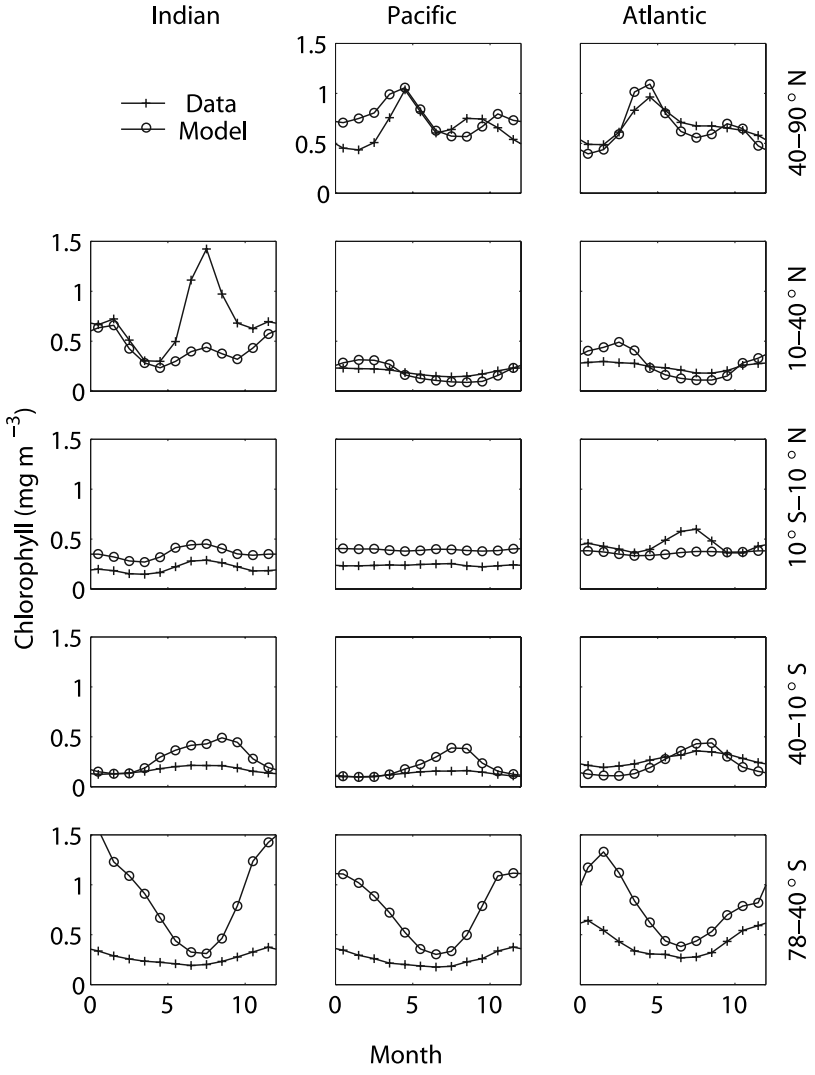

Figure 3. Modeled and observed surface chlorophyll in five latitude bands and the three major ocean basins.

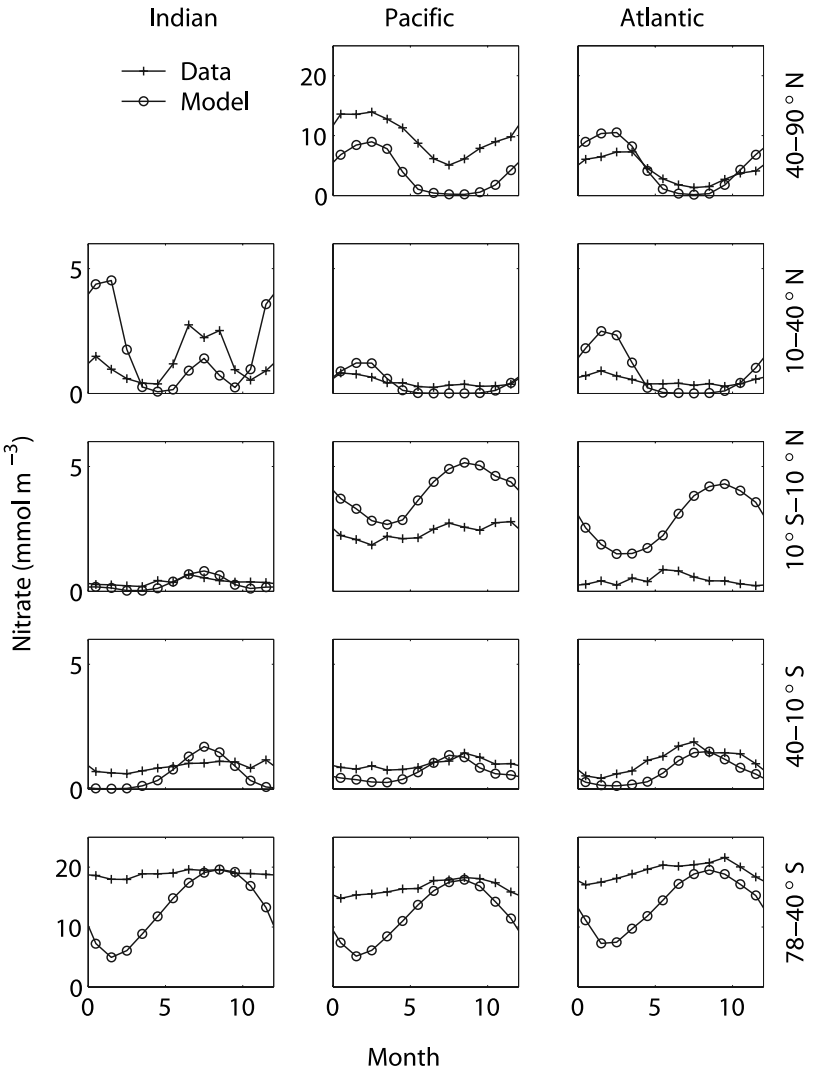

Figure 4. Modeled and observed surface nitrate in five latitude bands and the three major ocean basins. Note the change in scale at 40° latitude in both hemispheres.

progress in this area [e.g., *Hamme and Emerson*, 2006] but the data do not exist to evaluate parameterizations on large scales. For k_w, the formulation proposed by *Wanninkhof* [1992] for long-term winds is used:

$$k_w = (1-f)0.39\left(\frac{Sc_{O_2}}{660}\right)^{-1/2} u^2, \tag{4}$$

where k_w has units of cm hr^{-1}; f is the fraction of the sea surface covered with ice, diagnosed from the sea surface temperature according to *NCAR Oceanography Section* [1996]; Sc_{O2} is the Schmidt number for oxygen, computed using the formula of *Keeling et al.* [1998]; and u is the wind speed at 10 m in m s^{-1}, obtained from NCEP as in the physical model.

[11] In order to separate biotic and abiotic variations in the O_2 distribution, we define three forms of oxygen in the model: total oxygen (O_2^t), biological oxygen (O_2^b) and solubility oxygen (O_2^s). They have different air-sea fluxes, in situ sources and sinks, and initial conditions, as detailed in Table 2. All of the forms of oxygen are controlled by a similar transport-reaction equation:

$$\frac{\partial[O_2^i]}{\partial t} = \Pi([O_2^i]) + S(O_2^i), \tag{5}$$

where Π is the advective-diffusive transport operator (which is linear in $[O_2^i]$), the subscript i denotes the type of oxygen and S is the net in situ source of oxygen. From the above equation and the definitions in Table 2, it is straightforward to show that$[O_2^t] = [O_2^b] + [O_2^s]$. Note that $[O_2^s]$ is simply the oxygen concentration in the absence of biology and can differ from solubility equilibrium because of subsurface solar heating, mixing, and the finite kinetics of air-sea gas exchange. Note also that $[O_2^b]$ can be less than zero; conceptually it is similar to the negative of the apparent oxygen utilization (AOU) and generally decreases with depth.

[12] Quantifying the true air-sea flux of O_2^s is important for determining the biological contribution to the air-sea oxygen

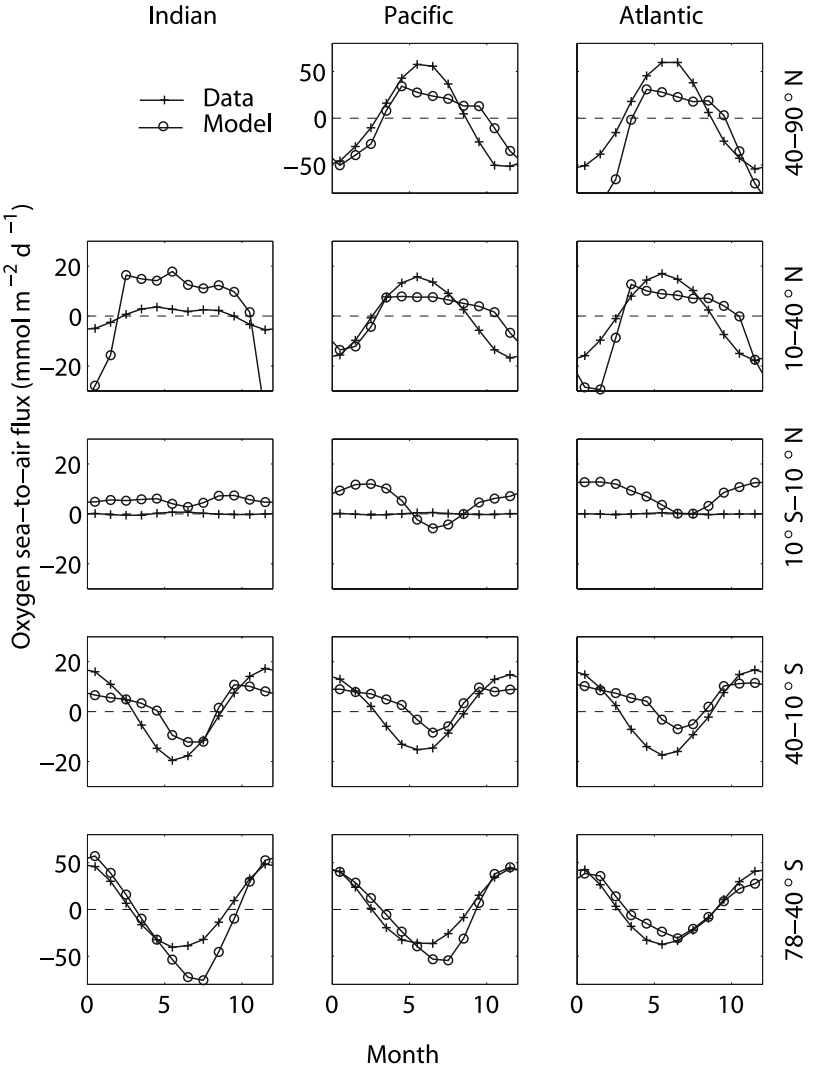

Figure 5. Modeled and observed departure of the sea-to-air oxygen flux from its annual mean in five latitude bands and the three major ocean basins. Note the change in scale at 40° latitude in both hemispheres.

flux, which should be more closely related to net community production than the total oxygen flux. Previous attempts to compute the air-sea flux of O_2^s have used estimates of the surface heat flux (because temperature is the dominant influence on solubility) and the assumption that the ocean stays close to equilibrium with the atmosphere [*Keeling et al.*, 1993]. The resulting relationship, which will be explored in this study, is

$$F_T^{Heat} = \frac{\partial [O_2^{sat}]}{\partial T} \frac{Q}{\rho C_p}, \tag{6}$$

where F_T^{Heat} is defined positive upward, Q is the total ice-free sea-to-air flux of heat (the total flux multiplied by $1 - f$), C_p is the specific heat of seawater (set to a constant value of 3993 J kg^{-1} K^{-1}) and ρ is the surface ocean density. We will evaluate the extent to which this formula approximates the air-sea oxygen flux resulting from the variation of oxygen solubility in the model.

2.4. Initialization and Integration

[13] The physical model was initialized with a spun-up state of the integration of the original NCOM model. This state was created by first running the model for 96 momentum years, 960 surface tracer years, and 9600 deep tracer years with the acceleration technique of *Bryan* [1984]. The integration was then continued for another 30 years with equal (synchronous) time steps.

[14] The initial nitrate and oxygen fields were taken from the climatologies of *Louanchi and Najjar* [2000] and *Najjar and Keeling* [1997], respectively. The initial chlorophyll and remaining nitrogen fields were set to constant values at the surface, decreasing exponentially with a scale depth of 100 m, similar to *Sarmiento et al.* [1993]. Initial surface concentrations were 0.14 mg m^{-3} for Chl, 0.14 mmol m^{-3} for P, 0.014 mmol m^{-3} for Z, and 0.1 mmol m^{-3} for NH_4,

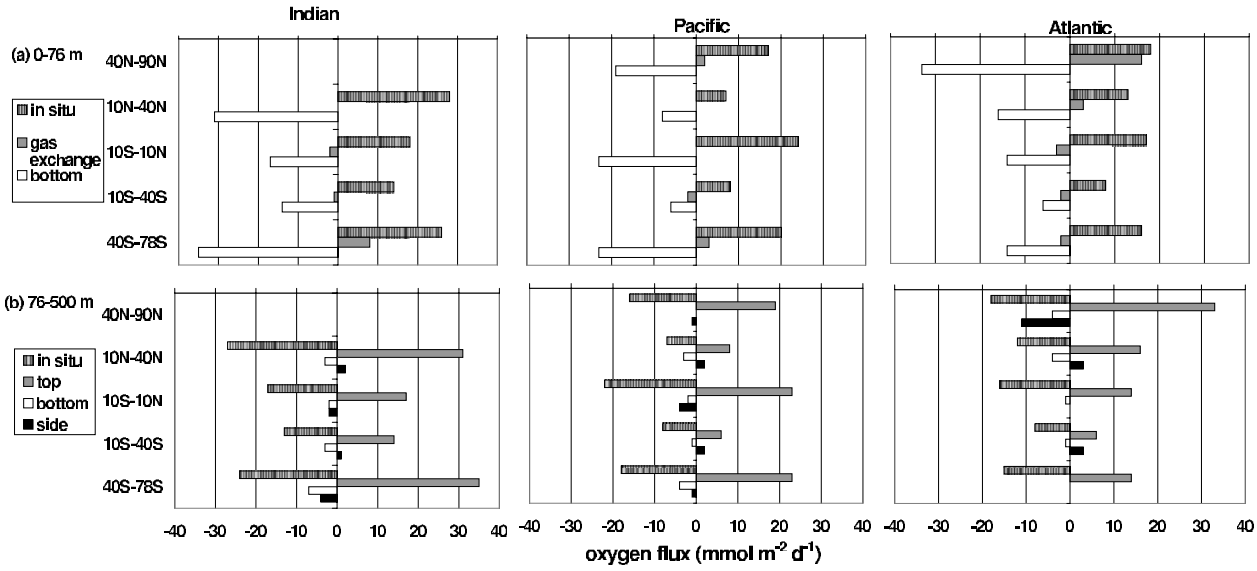

Figure 6. Annual mean budget of biological O_2 in the (a) production zone and (b) the consumption zone as a function of latitude band in each of the major ocean basins. Positive values are oxygen sources, and negative values are oxygen sinks.

DON and *D*. The biology was integrated with the evolving physical fields over an 11-year period. Our analysis is based on results from the eleventh year.

3. Model Evaluation

[15] In order to examine the model skill, we compare the model output with monthly climatologies of surface chlorophyll, surface nitrate and the air-sea oxygen flux. Chlorophyll is derived from the Sea-viewing Wide-Field-of-view Sensor (SeaWiFS) over the years 1997 to 2000, nitrate from the 2001 World Ocean Atlas [*Conkright et al.*, 2002], and the deviation from the annual mean O_2 flux from *Garcia and Keeling* [2001]. Basin-scale comparisons are used to investigate the overall features of seasonal variability of the model. Fourteen regions are defined by dividing the oceans by basin (Indian, Pacific, and Atlantic) and by broad latitude bands with boundaries at 40°S, 10°S, 10°N and 40°N, similar to *Conkright et al.* [1994] and *Gregg* [2002].

[16] Usually the ecosystem components in the surface will be in an approximate steady state after a few years run [*Sarmiento et al.*, 1993]. Figure 2 shows the air-sea oxygen flux averaged over each hemisphere as a function of time. With an 11-year biological run, the annual cycle has reached steady state. The global annual mean integrated air-to-sea O_2 flux in the model in the eleventh year is 0.8 mmol m^{-2} d^{-1}, which is at least an order of magnitude smaller than the amplitude of the annual cycle averaged over each hemisphere.

[17] Simulated chlorophyll is averaged over the upper 28 m, the top two layers in the model, representing one attenuation length for the satellite observations. As shown in Figure 3, the model picks up some of the features of the observations: elevated values and a large dynamic range in high latitudes, low values and moderate variability in the midlatitudes, and moderate values and small variability in the tropics. The model also captures the observed phasing of the annual cycle within a month or two in all of the regions. The magnitude and timing of the spring bloom in the high latitudes of the North Atlantic and Pacific is simulated reasonably well, as is the less pronounced fall bloom, though the timing is slightly off. In the North Indian Ocean, the model's chlorophyll maximum in response to the summer monsoon is too weak, at least partially because the coarse resolution of the model is not suitable for resolving upwelling during this time. This is consistent with nitrate levels being too low (Figure 4) and outgassing of oxygen too high (Figure 5) in the model during the summer. The model substantially overestimates both the mean and the amplitude of the annual chlorophyll cycle in the Southern Ocean, where the maximum is about three times greater than the observations while the minimum value in the model is comparable with the observations. The reason for the overestimation in the model may be that Fe limitation, which has been considered to play an important role in the Southern Ocean [*Boyd and Abraham*, 2001], is not present in our model. Iron limitation is also the likely explanation for the model's overestimate of chlorophyll in the equatorial Pacific [*Kolber et al.*, 2002] and possibly the equatorial Indian Ocean. Chlorophyll levels in high nitrate–low chlorophyll (HNLC) regions are captured better in some recent, more sophisticated marine ecosystem simulations that include iron limitation [e.g., *Moore et al.*, 2004].

[18] In subtropical regions, except in the North Indian Ocean, model chlorophyll is too low in the summer and too high in the winter. The summer deficit is likely due to the model's lack of mesoscale eddies, which have been shown to be an important source of nutrients in a number of oligotrophic environments [*Falkowski et al.*, 1991; *McGillicuddy et al.*, 1998]. This is consistent with lower than observed nitrate (Figure 4) and outgassing of oxygen (Figure 5) in the model during this time. Another possible reason for low chlorophyll

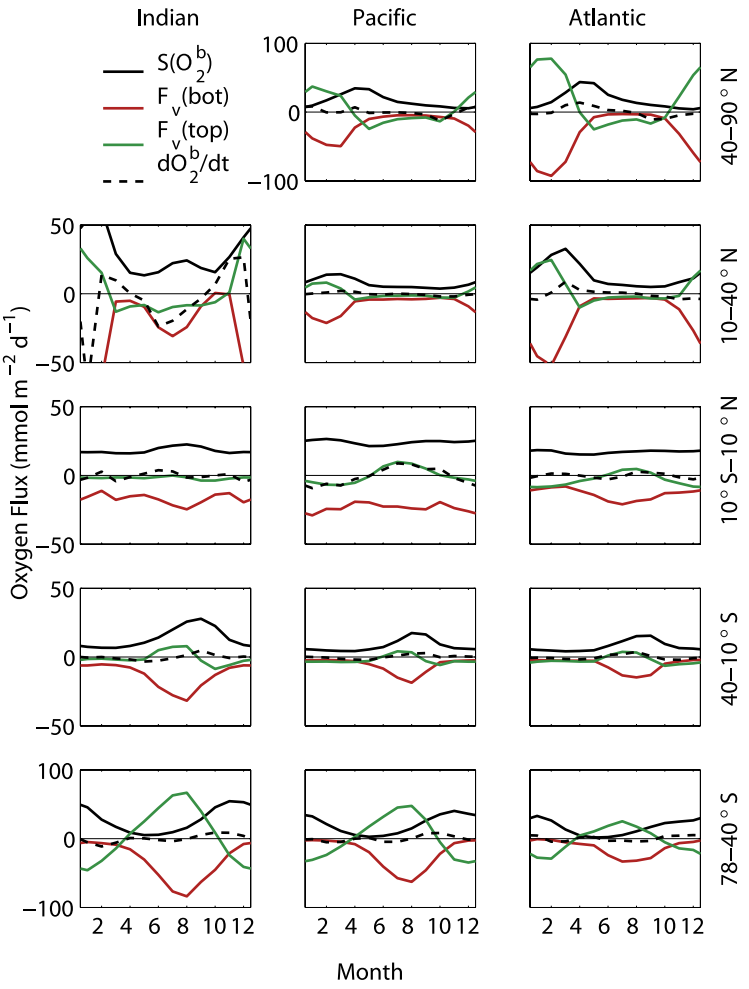

Figure 7. Seasonal budget of biological O_2 in the production zone as a function of latitude band in each of the major ocean basins. Note the change in scale at 40° latitude in both hemispheres.

is that the model does not include nitrogen fixation, which has been considered to be an important nitrogen source in subtropical gyres [*Capone et al.*, 2005]. The winter/spring chlorophyll excess may be due to higher than observed nitrate levels during winter (Figure 4), which may be related to the initialization with *Louanchi and Najjar* [2000]; this atlas likely overestimates subtropical nutrient levels because of the extensive smoothing in it. The winter/spring excess may also be due a lack of multiple phytoplankton species in the model; species succession has been shown to be an important feature of the spring bloom.

[19] As with the chlorophyll distribution, the model surface nitrate and air-sea O_2 flux fields capture the overall meridional pattern and temporal phasing of the observations even though there are substantial biases (Figures 4 and 5). Those biases seem to be consistent with the suspected causes of problems in the chlorophyll distribution, as already noted for the subtropics, including the North Indian Ocean. In the Southern Ocean, nutrient concentrations, though still saturating, are too low, presumably because biological production is too high. This results in the amplitude of the air-sea O_2 flux to be too large. A similar case can be made for the equatorial Pacific and Atlantic.

[20] In the North Atlantic, model errors are consistent between chlorophyll, nitrate and the air-sea O_2 flux in that the model slightly overestimates the amplitude of the annual cycle for all, while getting the mean in the first two about right. In the North Pacific, chlorophyll is slightly high, perhaps because the model does not include Fe limitation. This then results in too much production and nitrate levels that are too low. One would then expect the amplitude of the air-sea O_2 flux to be too large in the model, but this is not found.

[21] In summary, despite shortcomings, the model captures the large-scale behavior of surface nutrients and chlorophyll and the air-sea oxygen flux. Because we are more interested in relationships between biological rates and annual oxygen cycles rather than the absolute rates themselves, and because we suspect that those relationships are controlled by large scale physical processes that the circulation model is able to capture [*Large et al.*, 1997; *Doney et al.*, 1998], we believe the shortcomings are acceptable in this first attempt to link observed oxygen fluxes with net community production and remineralization.

4. Results and Discussion

4.1. Biological Oxygen Balance

[22] The ocean can be vertically separated into two different zones by the compensation depth, above which

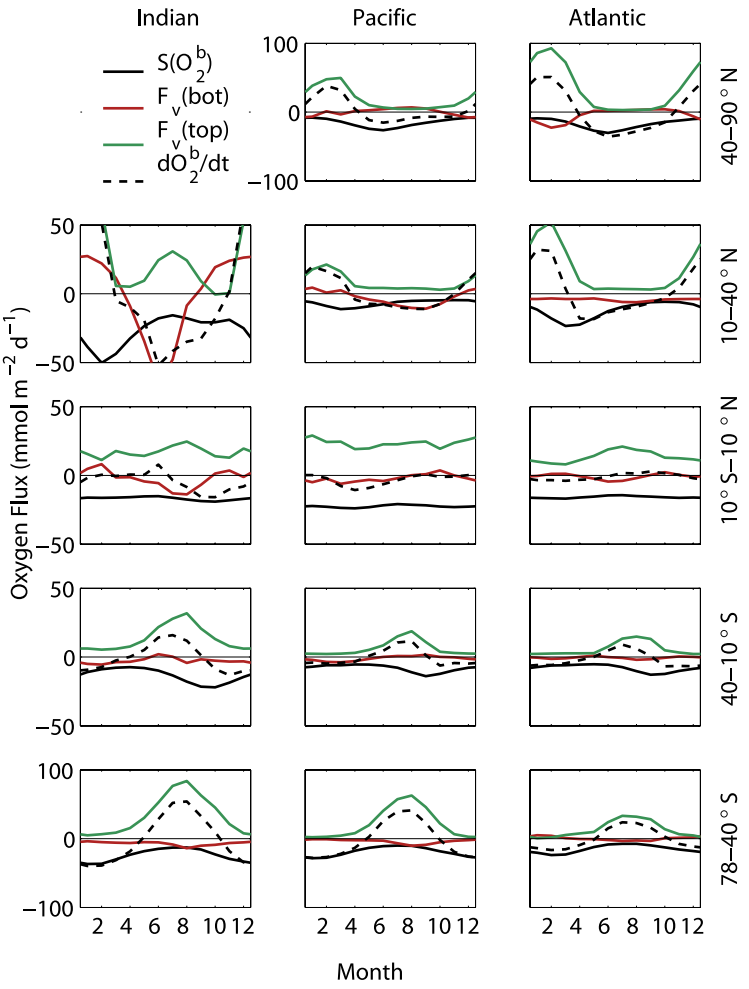

Figure 8. Seasonal budget of biological O_2 in the consumption zone as a function of latitude band in each of the major ocean basins. Note the change in scale at 40° latitude in both hemispheres.

the biological community is a net source of oxygen (O_2 production zone) and below which the biological community is a net sink of oxygen (O_2 consumption zone). For the purpose of simplicity, we ignore the seasonal variability of the compensation depth. On the basis of the global annual mean net biological production profile of the model (not shown), the compensation depth is chosen at the base of the fourth model layer, or about 76 m depth, which is in general agreement with that deduced from the analysis of dissolved oxygen observations [*Najjar and Keeling*, 1997]. The bottom depth of the O_2 consumption zone is chosen as 500 m because 95% of the organic matter exported from the surface ocean is remineralized above this depth in the model. The mass balance for biological O_2 in a given region of area A and volume V can be expressed as:

$$\frac{1}{A}\frac{\partial}{\partial t}\int_V [O_2^b]dV = F_v^{top} + F_v^{bot} + F_h + \frac{1}{A}\int_V S(O_2^b)dV, \qquad (7)$$

where F_v^{top}, F_v^{bot} and F_h are averages of the fluxes of biological O_2 across the top, bottom and sides of the zone, respectively.

4.1.1. Annual Mean

[23] Figure 6a shows the annual mean balance of biological O_2 in the production zone (0–76 m). Lateral fluxes and annual mean tendencies (i.e., model drift) are negligible in this zone, accounting for less than 2% of the biological source terms, and are not shown. The dominant balance is between production and downward transport of O_2 across the compensation depth. As expected from the large-scale pattern of vertical advection and mixing, O_2 production is highest in the tropics and high latitudes and lowest in the subtropics, except for the subtropical north Indian Ocean, which is very productive due to monsoonal circulation. The modest air-sea flux (except in the high latitudes of the North Atlantic) reveals a pattern of ingassing at high latitudes and outgassing at low latitudes, similar to previous calculations [*Najjar and Keeling*, 2000; *Gruber et al.*, 2001; *Ganachaud and Wunsch*, 2002]. The vertical fluxes across the compensation depth are all downward (Figure 6a) and are typically dominated by diffusion in middle to high latitudes and advection in the low latitudes (not shown); the former results from mixing acting on the decrease of $[O_2^b]$ with depth and the latter results from upwelling of water with negative $[O_2^b]$ levels.

[24] Figure 6b summarizes the annual mean O_2^b term balances in the O_2 consumption zone (76–500 m). Oxygen consumption, which very nearly equals the oxygen production above, is generally balanced by a downward vertical transport of oxygen across the compensation depth. The

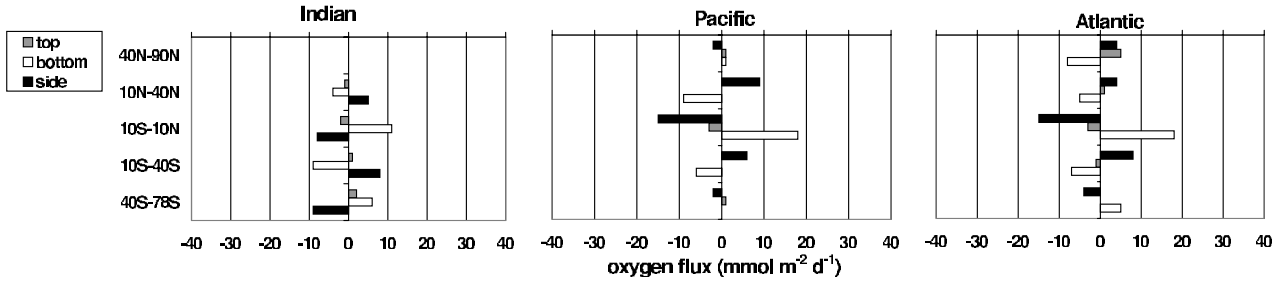

Figure 9. Annual mean budget of solubility O_2 in the production zone as a function of latitude band in each of the major ocean basins.

downward transport of biological oxygen across 500 m is generally small, but increases with latitude, as expected based on the corresponding decrease in stratification and increase in deep and intermediate water formation. Horizontal fluxes of biological oxygen are from high latitudes and the tropics into the midlatitudes; this is likely due to the lower branches of the Ekman circulation, which carry negative $[O_2^b]$ from midlatitudes both poleward and equatorward. In general, however, these horizontal biological oxygen fluxes are small. The exception occurs in the North Atlantic Ocean where horizontal transport of biological oxygen accounts for 60% of the biological oxygen sink.

4.1.2. Annual Cycle

[25] On the subbasin scale, the annual cycle of O_2^b in the production zone (0–76 m) is dominated by O_2 production and vertical exchanges with the consumption zone (76–500 m) and the atmosphere (Figure 7). The seasonal variation of horizontal transport is not shown because it is very small. Though the biological O_2 tendency in the model is generally small in the production zone, it is shown for later comparison with the tendency in the consumption zone, where it is significant.

[26] As expected from the model's annual cycle in chlorophyll and nutrients, the amplitude and phase of the annual cycle in biological oxygen production increase with latitude. At high latitudes, the biological oxygen annual cycles can be divided into four stages. In the winter, the deepening mixed layer causes an entrainment of oxygen-poor waters into the production zone (red lines in Figure 7), which creates a large oxygen demand on the atmosphere (green lines). In the spring, when the mixed layer shoals, the downward oxygen flux decreases and production (black lines) increases. These result in a decrease of the ingassing until a reversal of the air-sea flux occurs. Part of the oxygen produced during this time is fluxed into the air and the remainder is transported into the consumption zone. During the summer, as the mixed layer depth decreases, production decreases and almost equals outgassing. In the fall, production continues to decrease, and is either outgassed or transported into the consumption zone as a result of the decreasing stratification.

[27] The annual cycle is similar at middle latitudes, except that production peaks earlier and downward mixing is as significant as outgassing in balancing O_2 production. The subtropical north Indian Ocean is an exception, where there is a semiannual cycle in production that reflects monsoon-driven upwelling. Oxygen is ingassed during the winter, when upwelling and vertical mixing of O_2-depleted water is strong and light levels are inadequate to balance this with enhanced production. Vertical transport is weaker in the summer, and so more of the oxygen production can be outgassed. Seasonality in the zonal mean O_2 budget is relatively weak in the tropics, partly because much of the seasonality there is related to wind-driven east-west tilting of the pycnocline, and so is averaged out in our presentation.

[28] The O_2^b tendency in the consumption zone has significant seasonality in middle and high latitudes (Figure 8). Oxygen changes in the consumption zone are largely driven by consumption (a sink), which dominates the balance in the summer, and downward mixing across the compensation depth (a source), which dominates in winter. Vertical transport at 500 m is a relatively small term in the seasonal budget, except in summer, when it can rival in situ consumption in some regions. In spring and fall, consumption and downward mixing are nearly equal, resulting in little change in the O_2 concentration. Note that the O_2 consumption (Figure 8) closely mirrors the production above (Figure 7), with a lag (in the peak) of about 1 month at middle latitudes and 2 months at high latitudes, consistent with the time required for particles sinking at 5 m d^{-1} (Table A1) to travel a few hundred meters.

4.2. Solubility Oxygen Balance

4.2.1. Annual Mean

[29] In surface waters, fluxes of solubility oxygen in the annual mean are those expected from the Ekman circulation, with an upwelling source in the tropics, a downwelling sink in the subtropics, and an upwelling source at high latitudes, except in the North Atlantic, where the downwelling branch of the thermohaline circulation results in a solubility O_2 sink (Figure 9). These vertical fluxes are largely balanced by fluxes due to the lateral branches of the Ekman and thermohaline circulations. Vertical diffusion contributes little to the solubility O_2 balance, except in the North Atlantic, where it equals the advective flux (not shown). The small difference between the vertical and lateral water transports is made up by air-sea exchange, which acts as an oxygen sink in regions of net heating and a source where there is net cooling. Fluxes in the consumption zone (not shown) are dominated by a balance between lateral fluxes

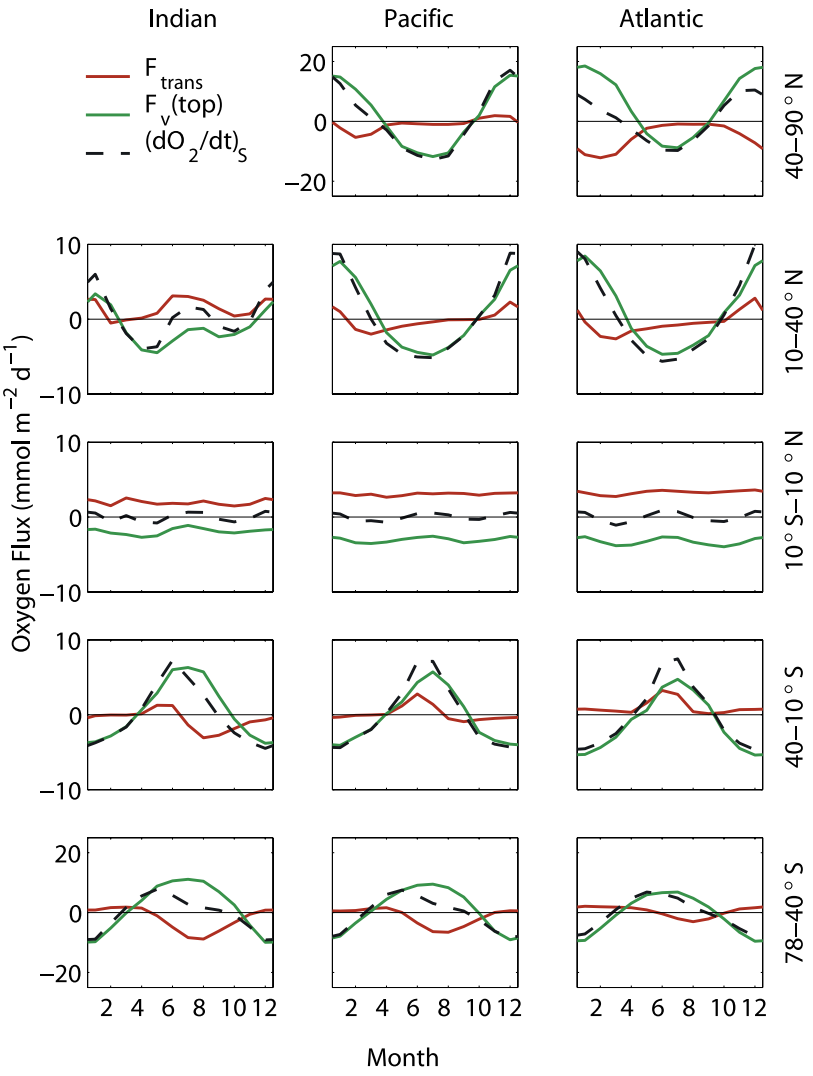

Figure 10. Seasonal budget of solubility O_2 in the production zone as a function of latitude band in each of the major ocean basins. Note change in scale at 40° in each hemisphere. F_{trans} is the sum of the fluxes at the sides and bottom of the zones.

and vertical fluxes at 76 m, except in high latitudes, where fluxes at 500 m become important.

4.2.2. Annual Cycle

[30] Given the close compensation of lateral and vertical water transports of solubility O_2 in the production zone, we have combined the two in the analysis of the seasonal budget (Figure 10). Solubility oxygen acts inversely to temperature: increasing in the winter and decreasing in the summer. This tendency is closely balanced by air-sea exchange, except in high latitudes during the winter, when downward mixing of oxygen is a significant sink. In the equatorial bands, seasonal variations are small and net outgassing is balanced by circulation.

[31] Figure 11 shows comparisons between the solubility O_2 sea-to-air fluxes calculated from the model heat fluxes, F_T^{Heat} (equation (6)), and the solubility O_2 sea-to-air fluxes in the model, F_T^{Model}. The annual cycles of F_T^{Heat} lead those F_T^{Model} and have larger amplitudes. We adjusted the phase and amplitude of F_T^{Heat} by trial and error until it gave a good visual agreement with F_T^{Model}; the result, shown in black in Figure 11, is given by

$$F_T(t) \approx \frac{1}{1.3} F_T^{Heat}(t - 0.5\text{mon}). \quad (8)$$

[32] The larger amplitude and lead of F_T^{Heat} with respect to F_T^{Model} is expected because of the finite rate of gas exchange, based on the box model of *Keeling et al.* [1993]. However, amplitude reduction factors of 1.3 to 1.5 correspond to time lags of 46 to 56 d in this box model, which is inconsistent with our results. A possible explanation for this discrepancy includes the effects of mixing and solar radiation penetrating below the mixed layer, which, according to *Dietze and Oschlies* [2005], each reduce the flux amplitude by about 10%. *Dietze and Oschlies* [2005] did not examine effects on the phase, but we suggest that these would be minimal. Penetrating solar radiation would be accounted for simply by reducing the net heat flux by the

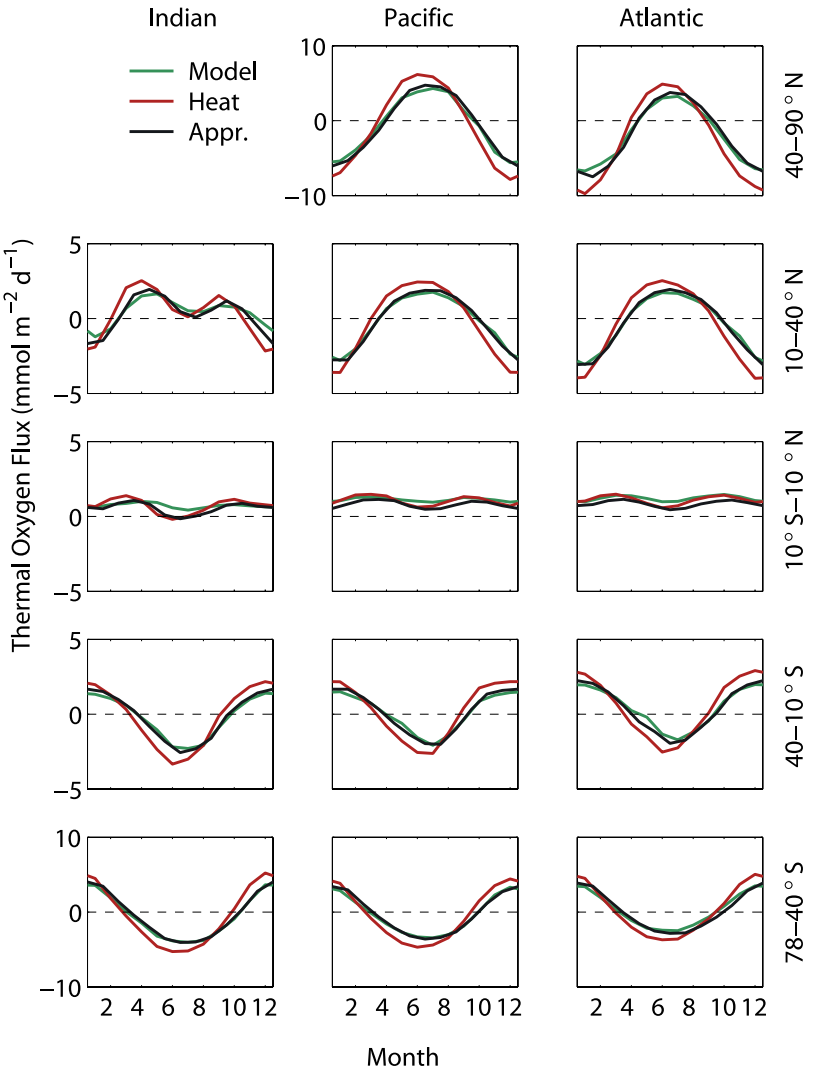

Figure 11. Seasonal variation of the solubility component of the sea-to-air oxygen flux in the model (green) and approximations of this flux using equations (6) (red) and (8) (black). Note change in scale at 40° in each hemisphere.

amount of downward radiation at the base of the mixed layer, which would mean a reduction in the thermally induced outgassing in the summer. Mixing, according to *Dietze and Oschlies* [2005], would effectively create an oxygen source to the mixed layer when it deepens during the fall and winter, which would counter ingassing at this time. Thus the corrections act out of phase with the flux and thus would not be expected to change the phase of the flux itself.

[33] Seasonal time series of upper ocean argon saturation [e.g., *Spitzer and Jenkins*, 1989] and atmospheric Ar/N_2 data [*Battle et al.*, 2003] have the potential for evaluating parameterizations of the thermally induced air-sea flux of oxygen. However, there are limitations to both types of data at the current time. For the oceanic Ar data, time series are limited to a few sites and the influence of bubbles needs to be removed. Atmospheric Ar/N_2 data are appealing because they integrate over large scales, and atmospheric simulations show good correspondence with observations when forced by air-sea fluxes estimated from heat flux, as in equation (6) [*Battle et al.*, 2003]. We believe, however, that measurement error, in addition to atmospheric transport model error, is likely too large at the current time to further refine air-sea flux parameterizations.

[34] As shown in Figure 12, solubility O_2 variations in the consumption zone are modest, generally less than 5 mmol m^{-2} d^{-1}, small compared to biological O_2 variations (Figure 8). To aid in the interpretation of these variations, we also present the time rate of change of the saturation concentration. In general, the two are similar. Solubility O_2 variations are most substantial at high latitudes, with decreases during the summer and increases during the winter, similar to changes in the saturation concentration (with a slight lag and reduced amplitude). Vertical diffusion dominates the time tendency (not shown). The cycle at middle latitudes is more complex, with summer increases (except in the North Atlantic) and winter decreases, and no amplitude reduction compared to the saturation concentration, though still lagging it. The small annual cycle at middle latitudes reflects both advection and vertical diffu-

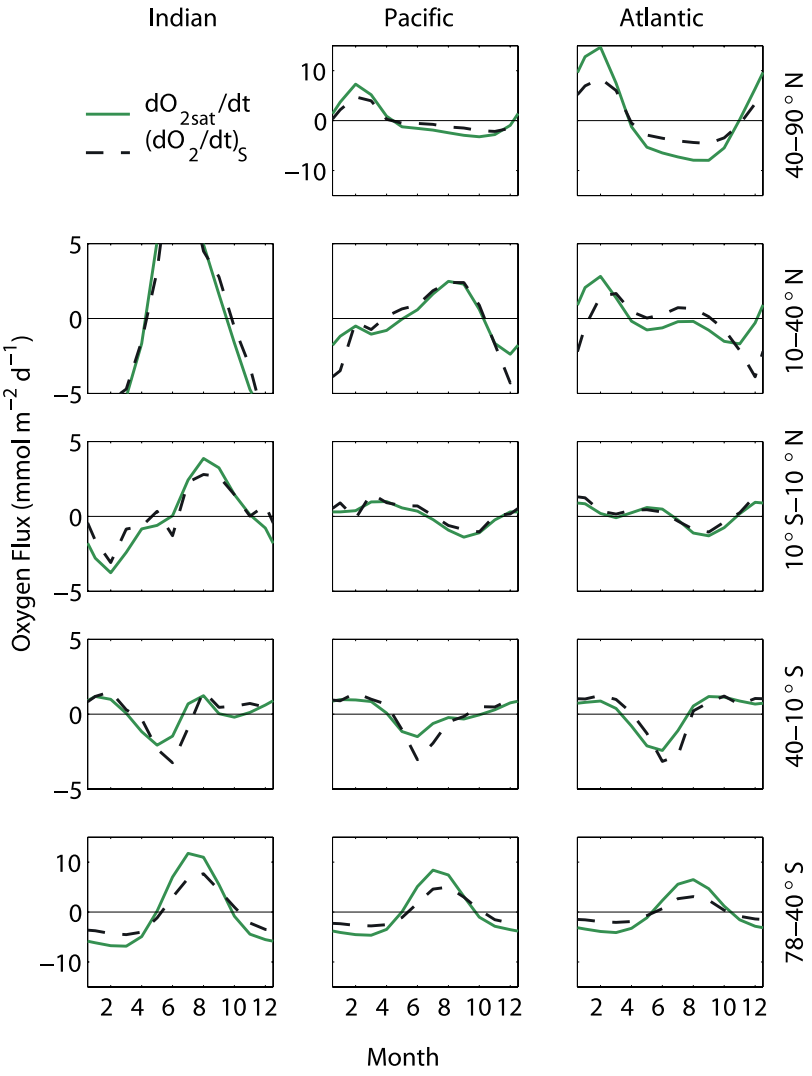

Figure 12. Seasonal budget of solubility O_2 in the consumption zone as a function of latitude band in each of the major ocean basins. Note change in scale at 40° in each hemisphere.

sion (not shown). The advection seasonality is consistent with that expected from Ekman pumping; the larger expected pumping rates in winter push shallower, warmer, O_2-depleted water downward, resulting in the observed negative tendencies. This is also supported by temperature observations in the Pacific between 10° and 40°N, which show negative seasonal anomalies on the order of 0.1°C at 150 and 250 m in the fall (October–December), as seen by *Antonov et al.* [1998, pp. 104, 106]. A temperature decrease of 0.1°C corresponds to an O_2 saturation concentration increase of about 0.5 mmol m^{-3}, which is roughly equal to the positive time tendency in Figure 12, after integrating with time and depth. Regardless of the cause of the variations in solubility O_2, it is clear that they are small and well approximated by variations in the saturation concentration. This means that changes in biological O_2 are essentially the same as changes in the oxygen anomaly ($O_2 - O_2^{sat}$), which was assumed by *Jenkins and Goldman* [1985] and *Najjar and Keeling* [2000].

4.3. Relationship of Net Community Production and Remineralization to Seasonal Oxygen Variations

[35] We now evaluate the relationship, in the biological O_2 simulation, of the seasonal net outgassing (SNO) of oxygen to net community production during the outgassing period and to annual net community production (Figure 13a). SNO here is computed by integrating the regional average surface fluxes shown in Figure 7 over the months of outgassing. Net community production (NCP) is simply defined as the volume integral of net oxygen production above 76 m. Though we present results for all 14 regions, we are primarily interested in the 10 regions in the middle and high latitudes outside of the north Indian Ocean (Table 3), where we expect seasonal variations in the oxygen cycle to be more closely linked to biological rates. The fraction of annual NCP that occurs during the outgassing period is greater at higher latitudes (range 0.62 to 0.78, median 0.73) than at middle latitudes (range 0.43 to 0.65, median 0.63), reflecting the fact that (at least in the model) light limits production in the former and nutrients in the latter. This difference in limitation

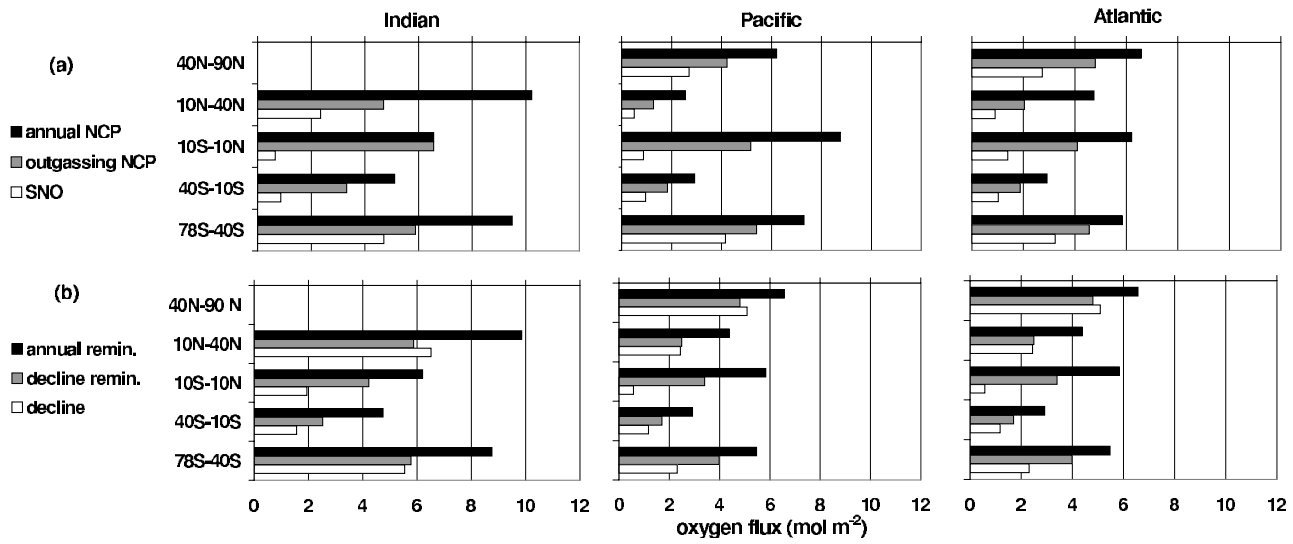

Figure 13. (a) Annual net community production, net community production during the O_2^b outgassing period, and seasonal net outgassing of O_2^b as a function of latitude band in each of the major ocean basins. (b) Annual remineralization, remineralization during the period of O_2^b decline, and the total O_2^b decline in the consumption zone as a function of latitude band in each of the major ocean basins.

leads to earlier peaks in production (i.e., the spring bloom) at middle latitudes (Figure 7) [*Siegel et al.*, 2002]. The ratio of SNO to NCP during the outgassing period also is greater at higher latitudes. This, too, presumably reflects the difference in growth limitation between the two regions; where nutrients limit growth, an increasing fraction of production occurs at greater depths, below the mixed layer, leaving more of the oxygen available for seasonal storage and downward mixing instead of outgassing. Overall, the fraction of annual NCP that is outgassed is relatively small: 0.17 to 0.35 (median 0.20) at middle latitudes and 0.42 to 0.58 (median 0.50) at high latitudes.

[36] In the biological O_2 simulation, there are similar latitudinal differences in the relationship between the thermocline oxygen decline (TOD) and remineralization in the consumption zone. Figure 13b and Table 4 show that the fraction of annual remineralization that occurs during the oxygen decline is slightly lower at middle latitudes (range 0.53–0.63, median 0.57) than at high latitudes (range 0.66–0.75, median 0.73). This trend is also likely a function of the earlier spring bloom at midlatitudes, which results in remineralization occurring while stratification is still weak, leaving much of the O_2 consumption balanced by downward mixing and thus not reflected in O_2 decreases (Figure 8). The ratio of the TOD itself to remineralization shows no obvious relationship to latitude, ranging from 0.59 to 1.12 at middle latitudes and 0.52 to 1.06 at high latitudes. Overall, the TOD is a similar fraction of annual remineralization at middle (range 0.33–0.71, median 0.40) and high (range 0.35 to 0.77, median 0.42) latitudes.

4.4. Application to Observed Flux Estimates

[37] We now apply the ratios in Tables 3 and 4 to observed estimates of seasonal outgassing and thermocline drawdowns of oxygen from observations. We use the *Josey et al.* [1998] monthly heat flux climatology to estimate F_T^{Heat} according to equation (6), average those fluxes within each of the 10 regions, and then apply the correction based on equation (8). The lag of two weeks in equation (8) was applied for a given month simply by taking the average of F_T^{Heat} for that month and the previous month. This gives us an estimate of the observed thermally induced oxygen flux averaged over each region. We estimate the actual air-sea flux of biological O_2 by subtracting the thermal oxygen flux estimate from the total air-sea O_2 flux estimate of *Garcia and Keeling* [2001]. SNO for each region is estimated as was done for the model. For the consumption zone, we use the O_2 anomaly (-AOU) from *Conkright et al.* [2002]. We therefore ignore the differences between the tendencies in O_2^s and O_2^{sat} in the thermocline (Figure 12), which are very small compared to O_2^b tendencies (Figure 8). The biological TOD is taken to be twice the amplitude of a sinusoidal fit to the O_2 anomaly integrated between 75 and 500 m. To compute net community production (during O_2^b outgassing and annual) and remineralization (during the O_2^b decline and annual), we simply take the model-derived ratios for each

Table 3. Model Relationships Between Net Community Production During Outgassing, Annual NCP, and Seasonal Net Outgassing

	NCP During Outgassing ÷ Annual NCP			SNO ÷ NCP During Outgassing			SNO ÷ Annual NCP		
Region	Indian	Pacific	Atlantic	Indian	Pacific	Atlantic	Indian	Pacific	Atlantic
40°–90°N	-	0.68	0.73	-	0.64	0.57	-	0.44	0.42
10°–40°N	-	0.50	0.43	-	0.40	0.45	-	0.20	0.19
40°–10°S	0.65	0.63	0.64	0.26	0.52	0.55	0.17	0.33	0.35
78°–40°S	0.62	0.74	0.78	0.80	0.77	0.71	0.50	0.57	0.55

Table 4. Model Relationships Between Remineralization During the Thermocline Oxygen Decline, Annual RM, and the TOD

	RM During Decline ÷ Annual RM			TOD ÷ RM During Decline			TOD ÷ Annual RM		
Region	Indian	Pacific	Atlantic	Indian	Pacific	Atlantic	Indian	Pacific	Atlantic
40°–90°N	-	0.69	0.74	-	0.52	1.06	-	0.35	0.78
10°–40°N	-	0.63	0.55	-	1.12	0.98	-	0.71	0.56
40°–10°S	0.52	0.55	0.57	0.62	0.59	0.69	0.33	0.33	0.40
78°–40°S	0.66	0.74	0.74	0.96	0.84	0.58	0.63	0.63	0.42

region (last six columns of Tables 3 and 4) and apply them to the observed estimates of biological SNO and TOD.

[38] We make a rough estimate of the error by considering individual, uncorrelated errors in SNO, TOD, and the ratios of the O_2 fluxes to the rates of interest (Tables 3 and 4). *Garcia and Keeling* [2001] find that amplitude errors in simulations of atmospheric O_2/N_2 with their flux climatology are on the order of 10%, and we adopt this error for SNO in each of the 10 regions. The error in TOD is taken to be the RMS error of the sinusoidal fit. We assume the same error in the ratios for all five midlatitude regions, and take it to be half the range. We do the same for all five high-latitude regions. For example, the error in the ratio of the TOD to remineralization in mid latitudes is $(0.71-0.33) \div 2 = 0.19$.

[39] SNO and NCP results are shown in Table 5. Excluding the tropics and north Indian Ocean, we find biological SNO to be 530 ± 18 Tmol O_2, where the error is estimated assuming that errors in each region (10%) are uncorrelated (i.e., the total error is the square root of the sum of the squares of individual errors). Our estimate of biological SNO is about 30% larger than that of *Garcia and Keeling* [2001]. We expect a larger value because we do not assume instantaneous equilibrium when computing thermal SNO. The magnitude of the difference is as expected as well, given the similar values of thermal and biological SNO estimated by *Garcia and Keeling* [2001], but differences could also arise from the different estimates of heat flux, winds, and oxygen concentration, as well as the different spatial aggregation.

[40] Excluding the tropics and north Indian Ocean, NCP during the outgassing period is 940 ± 107 Tmol O_2, or 7.8 ± 1.4 Pg C using a C:O_2 ratio of 0.690 ± 0.092 [*Anderson and Sarmiento*, 1994]. *Lee* [2001] estimated export production during the period of seasonal warming (similar to our outgassing period) to be 6.7 ± 2.7 to 8.0 ± 2.7 Pg C, using seasonal drawdowns of dissolved inorganic carbon, with corrections for mixing and air-sea exchange. This agrees well with our estimate. The tropics and north Indian Ocean were included in Lee's estimates, but the seasonal nature of the calculation likely results in a substantial underestimate in these areas, particularly in the tropics, where upwelling occurs throughout the year.

[41] We estimate annual NCP outside the tropics and the north Indian Ocean to be 1487 ± 193 Tmol O_2 or 12.3 ± 2.3 Pg C. This compares favorably with the annual estimates of *Lee* [2001], based on his seasonal estimates and scaling relationships using time series data: 9.1 ± 2.7 to 10.8 ± 2.7 Pg C. In order to estimate NCP globally, we use new production estimates for upwelling areas from *Chavez and Toggweiler* [1995]. They estimated annual new production in the tropics (15°S to 15°N) to be approximately 2.2 Pg C. Monsoonal areas, mainly the north Indian Ocean, were estimated to export 0.4 Pg C yr^{-1}. No error estimates were given and so we subjectively give the summed export an error of 50%. We then arrive at a global NCP estimate of 14.9 ± 2.5 Pg C yr^{-1}. This is in agreement with the satellite-based estimate of export production made by *Laws et al.* [2000], 12 ± 0.9 Pg C yr^{-1}. *Gnanadesikan et al.* [2004] estimated a global particle export of 11 ± 1 Pg C yr^{-1} using the satellite-based algorithm of *Dunne et al.* [2005]. To compare with our global estimate, dissolved organic carbon (DOC) export must be considered. *Hansell* [2002] summarized net DOC production estimates in the euphotic zone and net DOC consumption estimates in the aphotic zone. Surface net DOC production is about 17% of export production, and DOC consumption is 20 ± 10% of remineralization. Both estimates are similar, and we use the latter to amend the *Gnanadesikan et al.* [2004] particle export to estimate a global export production of 13 ± 1 Pg C yr^{-1}, which also agrees with this study. Finally, we note that the simulations of *Gnanadesikan et al.* [2004] that are most consistent with hydrography (their P2 and P2A simulations) yield a global export of 14.4 and 15.6 Pg C yr^{-1}, which also agrees well with our estimate.

[42] Thermocline oxygen decline and remineralization results are shown in Table 6. Excluding the tropics and north Indian Ocean, the decline of biological O_2 between 75 and 500 m is 481 ± 48 Tmol O_2, which, on average, is 78% of remineralization during the decline and 49% of annual remineralization. Our estimate of the seasonal decline of O_2^b is 61% of the estimate made by *Najjar and Keeling* [2000], who used a different oxygen climatology than *Conkright et al.* [2002], a different method of integration (based on amplitudes of sinusoids at each depth level) and different

Table 5. Biological SNO and Net Community Production Estimates Using Ratios in Table 3[a]

	SNO				NCP During Outgassing				Annual NCP			
	Indian	Pacific	Atlantic	World	Indian	Pacific	Atlantic	World	Indian	Pacific	Atlantic	World
40°–90°N	-	68 ± 7	64 ± 6	132 ± 9	-	106 ± 22	113 ± 25	219 ± 33	-	156 ± 37	154 ± 39	310 ± 54
10°–40°N	-	43 ± 4	26 ± 3	69 ± 5	-	108 ± 41	59 ± 20	167 ± 46	-	216 ± 94	138 ± 59	354 ± 111
40°–10°S	37 ± 4	39 ± 4	20 ± 2	96 ± 6	144 ± 82	74 ± 22	35 ± 10	253 ± 85	222 ± 131	118 ± 41	55 ± 18	395 ± 138
78°–40°S	82 ± 8	97 ± 10	52 ± 5	231 ± 14	102 ± 18	126 ± 23	73 ± 14	301 ± 33	165 ± 36	170 ± 36	93 ± 20	428 ± 55
78°S–90°N	119 ± ± 9	247 ± 13	162 ± 9	528 ± 18	246 ± 84	414 ± 56	280 ± 36	940 ± 107	387 ± 136	660 ± 115	440 ± 76	1487 ± 193

[a]Units are Tmol.

Table 6. Thermocline Oxygen Declines and Remineralization Estimates Based on Ratios in Table 4[a]

	TOD				RM During Decline				Annual RM			
	Indian	Pacific	Atlantic	World	Indian	Pacific	Atlantic	World	Indian	Pacific	Atlantic	World
40°–90°N	-	49 ± 14	63 ± 4	112 ± 15	-	93 ± 55	59 ± 16	152 ± 57	-	136 ± 80	80 ± 21	216 ± 83
10°–40°N	-	91 ± 23	22 ± 8	113 ± 24	-	82 ± 28	22 ± 10	104 ± 30	-	130 ± 46	40 ± 19	170 ± 50
40°–10°S	34 ± 11	52 ± 19	32 ± 9	118 ± 24	55 ± 30	89 ± 51	46 ± 22	190 ± 63	106 ± 59	161 ± 94	80 ± 39	347 ± 117
78°–40°S	81 ± 24	27 ± 17	30 ± 9	138 ± 31	85 ± 35	32 ± 23	53 ± 29	170 ± 51	129 ± 53	43 ± 31	71 ± 40	243 ± 73
78°S–90°N	115 ± 26	219 ± 37	147 ± 16	481 ± 48	140 ± 46	296 ± 83	180 ± 41	616 ± 103	235 ± 79	470 ± 135	271 ± 63	976 ± 169

[a]Units are Tmol.

spatial aggregation (10° latitude bands). One expects a difference of this sign because of the change in phase with depth of the annual cycle [*Najjar and Keeling*, 1997]. Unlike the air-sea flux climatology, which used heat flux estimates for interpolation, and which has been corroborated with atmospheric O_2/N_2 measurements [*Battle et al.*, 2006], the AOU climatology likely suffers from inadequate sampling of the annual cycle, particularly in the Southern Hemisphere [*Najjar and Keeling*, 1997]. Outside the tropics and north Indian Ocean, remineralization during the decline and annual remineralization are estimated to be 5.1 ± 1.1 and 8.1 ± 1.8 Pg C, respectively. The latter is lower than the corresponding estimate of export production (12.3 ± 2.3 Pg C), possibly because of inadequate resolution of the AOU annual cycle and remineralization below 500 m.

[43] There are few large-scale estimates of remineralization with which to compare our results with. *Feely et al.* [2004] used oxygen and chlorofluorcarbon measurements from 24 cruises in the Pacific Ocean to estimate oxygen utilization rates. They find that the upper water column (200–1600 m) of the Pacific Ocean supports 5.3 ± 1 Pg C yr^{-1} of remineralization. This is comparable with our estimate for the Pacific, 3.9 ± 1.2 Pg C yr^{-1}, considering the 1–2 Pg C of export production in the tropics [*Chavez and Toggweiler*, 1995], our undersampling of the annual cycle, and remineralization below 500 m.

5. Conclusions

[44] Measurements of seasonal variations in atmospheric O_2/N_2, first reported by *Keeling and Shertz* [1992], gave oceanographers a unique, hemispherically integrated view of net community production at middle and high latitudes. However, there were at least three significant uncertainties in relating the annual oxygen cycle to export production: (1) the relationship between the air-sea oxygen flux and the annual O_2/N_2 cycle in the atmosphere, (2) the biologically induced portion of the air-sea flux, and (3) the relationship between the biological oxygen flux and export production. Here we have exploited a numerical model of marine oxygen variations to reduce the latter two uncertainties. We find that we can accurately remove the nonbiological portion of the air-sea flux in our model by reducing the equilibrium flux (computed from the temperature dependence of oxygen solubility and the surface heat flux) by 30% and introducing a lag of about two weeks. This implies that previous estimates of biological SNO based on the difference between total and thermal SNO are upwardly biased (also by about 30% because of the rough equivalence between the two components). We also find that extratropical (and outside the north Indian Ocean) seasonal outgassing of oxygen is, on average, 56% of net community production during outgassing and 35% of annual net community production. The first uncertainty listed above has been reduced using atmospheric transport models [*Keeling et al.*, 1998; *Garcia and Keeling*, 2001; *Battle et al.*, 2006], though our work suggests that, like the thermal O_2 flux, the thermal N_2 flux has probably been significantly overestimated.

[45] We have taken a similar approach to the seasonal thermocline drawdown in oxygen, which was first used to estimate open ocean remineralization by *Jenkins and Goldman* [1985] (locally) and *Najjar and Keeling* [2000] (globally). We find that the influences of oxygen solubility on seasonal O_2 trends are readily removed by using the saturation concentration, which means that seasonal trends in biological oxygen are essentially the same as those in the oxygen anomaly. Further, we find that the drawdown of the oxygen anomaly within the seasonal thermocline is 78% of the remineralization during the drawdown and 49% of annual remineralization.

[46] Our work is limited by deficiencies in the numerical model, such as the lack of mesoscale eddies and nitrogen fixation, which likely lead to underestimates of summertime production (and hence oxygen outgassing) in subtropical regions, and the lack of iron limitation, which may result in overestimates of summertime production and outgassing in some regions. Uncertainty in the parameterization of diapycnal mixing also influences exchange of oxygen and nutrients across the base of the mixed layer and euphotic zone. Thus it is likely that the sensitivity seen in annual mean distributions of nutrients, oxygen and export production to vertical and horizontal mixing [*Gnanadesikan et al.*, 2002, 2004] extends to the seasonal timescale. Mixing will further influence the relationship between heat flux and the thermally induced oxygen flux. Specifically, the greater the mixing, the smaller the seasonal amplitude of the thermally induced oxygen flux because (1) the longer the equilibration timescale with the atmosphere and (2) the greater the nonlinear mixing effect identified by *Dietze and Oschlies* [2005]. Finally, we have ignored interannual variations in dissolved oxygen, which can be appreciable in both the production and consumption zones [*Emerson*, 1987; *Deutsch et al.*, 2005]. The approach, however, of using models to relate seasonal variability in oxygen to rates of organic matter export and decomposition, is valuable, we believe, and should be attempted using more comprehensive marine ecosystem [e.g., *Moore et al.*, 2004; *LeQuéré et al.*, 2005] and circulation [e.g., *Dietze and Oschlies*, 2005] models and applied to interannual variations in atmospheric O_2/N_2 [*Bender et al.*, 1996]. Future modeling studies would also benefit from a greater focus on the mixed layer and the

Table A1. Ecosystem Model Parameters[a]

Parameter	Symbol	Value	Units
Phytoplankton Coefficients			
Initial slope of P^B–I curve	α	0.05	mmol N (mg chl)$^{-1}$ d^{-1} m^2 W^{-1}
Maximum chlorophyll a to nitrogen ratio	θ_m	4.5	mg Chl (mmol N)$^{-1}$
Activation energy	e_a	4.5	10^4 J mol^{-1}
Gas constant	R	8.3	J mol^{-1} K^{-1}
Phytoplankton aggregation coefficient	m_p	0.1	mmol^{-1} m^3 d^{-1}
Phytoplankton excretion rate constant	λ_p	0.075	d^{-1}
Nitrate half-saturation constant	k_{NO3}	0.5	mmol m^{-3}
Ammonium half-saturation constant	k_{NH4}	0.03	mmol m^{-3}
Phytoplankton maximal growth rate at 20°C	$\mu_p^{\max}(T_0)$	2	d^{-1}
Zooplankton Coefficients			
Half-saturation constant for grazing	ε	0.6	mmol m^{-3}
Assimilated fraction of phytoplankton	a_p	0.75	
Zooplankton maximal growth rate at 20°C	$\mu_z^{\max}(T_0)$	2	d^{-1}
Zooplankton excretion rate constant	λ_z	0.06	d^{-1}
Zooplankton mortality rate constant	m_z	0.4	mmol^{-1} m^3 d^{-1}
Dissolved fraction of excretion/mortality	γ	0.5	
Other Coefficients			
Nitrification rate constant[b]	λ_n	0.2	d^{-1}
DON ammonification rate constant[c]	λ_o	0.03	d^{-1}
DON/NH_4 excretion ratio[c]	f_n	0.7	
Detritus sedimentation speed[d]	V_d	5	m d^{-1}
Detritus solubilization rate constant[d]	λ_d	0.05	d^{-1}

[a]All parameters are from *Doney et al.* [1996], with a few adjustments based on the model behavior, except where noted.
[b]*Olson* [1981]. Set to zero above 76 m.
[c]*Foujols et al.* [2000].
[d]*Oschlies et al.* [2000].

seasonal thermocline, as opposed to the fixed depth intervals used in this study.

Appendix A: Ecosystem Model Description

[47] The net biological source for each of the seven components is given by

$$\begin{aligned}
S(P) &= \mu_p P - \mu_z Z - \lambda_p P - m_p P^2 \\
S(Z) &= a_p \mu_z Z - \lambda_z Z - m_z Z^2 \\
S(D) &= (1 - a_p)\mu_z Z + m_p P^2 + (1 - \gamma)\left(\lambda_z Z + m_z Z^2\right) \\
&\quad - \lambda_d D - V_d \partial_z D \\
S(DON) &= (1 - f_n)\left[\lambda_p P + \gamma\left(\lambda_z Z + m_z Z^2\right)\right] + \lambda_d D - \lambda_0 DON \\
S(NO_3) &= -\mu_p q_{NO_3} P + \lambda_n NH_4 \\
S(NH_4) &= -\mu_p q_{NH_4} P + f_n\left[\lambda_p P + \gamma\left(\lambda_z Z + m_z Z^2\right)\right] \\
&\quad + \lambda_0 DON - \lambda_n NH_4 \\
S(Chl) &= \mu_p P \rho_{chl} - \theta\left(\mu_z Z + \lambda_p P + m_p P^2\right),
\end{aligned}$$

where μ_p is the phytoplankton specific growth rate, μ_z is the zooplankton specific growth rate, ρ_{chl} is the ratio of chlorophyll a synthesis to nitrogen uptake, θ is the phytoplankton chlorophyll a:nitrogen ratio (Chl/P), q_{NH4} and q_{NO3} are the nitrate and ammonium fractions of phytoplankton nitrogen uptake, respectively, and the other symbols are defined in Table A1.

[48] The phytoplankton specific growth rate is expressed as a function of the irradiance and the chlorophyll a:nitrate ratio as follows [*Geider et al.*, 1997]:

$$\mu_p = \mu_p^m\left(1 - e^{-\alpha I_{par}\theta/\mu_p^m}\right),$$

where μ_p^m is the light-saturated phytoplankton specific growth rate, α is the initial slope of the chlorophyll-normalized photosynthesis-irradiance curve, and I_{par} is the downwelling irradiance in the photosynthetically active radiation (PAR) band (350–700 nm).

[49] We have used a constant ratio to transfer a carbon-based variable to a nitrogen-based variable. μ_p^m is considered to be a product of a nutrient limitation function $L(N)$ and a temperature dependent of function, $\mu_p^{\max}(T)$:

$$\mu_p^m = \mu_p^{\max}(T) L(N).$$

[50] The former is given as an Arrhenius temperature dependence:

$$\mu_p^{\max}(T) = \mu_p^{\max}(T_0) \exp\left[-\frac{e_a}{R}\left(\frac{1}{T + 273.15} - \frac{1}{T_0 + 273.15}\right)\right],$$

where $\mu_p^{\max}(T_0)$ is the maximum specific growth rate at reference temperature T_0 (293 K) under light-and-nutrient-replete conditions, and e_a/R is the slope of an Arrhenius plot.

[51] Nutrient limitation follows *O'Neill et al.* [1989] kinetics. On the basis of the work by *Fasham* [1995] we have

$$L_{NH_4} = \frac{NH_4}{k_{NH_4}(1 + NO_3/k_{NO_3} + NH_4/k_{NH_4})}$$

$$L_{NO_3} = \frac{NO_3}{k_{NO_3}(1 + NO_3/k_{NO_3} + NH_4/k_{NH_4})},$$

where L_{NH_4} and L_{NO_3} represent nitrate and ammonium limitation, respectively, and k_{NH_4} and k_{NO_3} are the half-saturation constants for ammonium and nitrate, respectively. Nitrogen uptake is partitioned between nitrate and ammonium as follows:

$$q_{NO_3} = \frac{L_{NO_3}}{L_{NO_3} + L_{NH_4}}$$
$$q_{NH_4} = \frac{L_{NH_4}}{L_{NO_3} + L_{NH_4}}.$$

[52] ρ_{chl} is assumed to be regulated by the ratio of achieved-to-maximum potential photosynthesis [*Geider et al.*, 1997]:

$$\rho_{chl} = \theta_m \left(\frac{\mu_p}{\alpha I_{par} \theta} \right),$$

where θ_m is the maximum chlorophyll a:N ratio observed in cells acclimated to extremely low light. ρ_{chl} declines when the instantaneous light harvesting capacity (i.e., $\alpha I_{par}\theta$) exceeds the instantaneous photosynthesis rate.

[53] I_{par} at the surface is specified as a fixed fraction (0.45) of total surface insolation, $E(0)$, which is taken from a spatially varying monthly climatology derived from the International Satellite Cloud Climatology Project [*Bishop and Rossow*, 1991]. The diurnal cycle is not resolved. A constant ocean albedo of 7% is applied to the downward short-wave flux, which decreases exponentially with depth with a constant attenuation coefficient k_{par}. The empirical relationship of *Morel* [1988] between $k_{par.}$ and the mean chlorophyll concentration ($\overline{Chl}$) within the euphotic zone (of depth z_e) is used. The equations are:

$$I_{par} = (0.45)(0.93)E(0)e^{-\kappa_{par} z}$$
$$\kappa_{par} = 0.121 \overline{Chl}^{0.428},$$

where k_{par} has units of m^{-1} and $\overline{Chl}$ has units of mg m^{-3}. The euphotic zone depth in m is computed from

$$z_e = 38.0 \overline{Chl}^{0.428}.$$

z_e and $\overline{Chl}$ depend on each other, so they are computed iteratively.

[54] For zooplankton grazing we use a type II grazing form

$$\mu_z = \mu_z^{\max} \frac{P^2}{\varepsilon^2 + P^2},$$

where $\mu_z^{\max}$ is the maximum specific grazing rate at temperature T and $\mu_z^{\max}$ has the same temperature dependence as $\mu_p^{\max}$, with the maximum specific grazing rate at T_0 given by $\mu_z^{\max}(T_0)$; ε is the grazing half-saturation constant.

[55] **Acknowledgments.** R.N., X.J., and F.L. were supported from the following grants: NOAA NA16GP2987, NASA NAG5-6451, and NSF OCE-9711937. We thank Hernan Garcia, Michael Bender, Ralph Keeling, and two anonymous reviewers for their comments.

References

Anderson, L. A. (1995), On the hydrogen and oxygen content of marine phytoplankton, *Deep Sea Res., Part I*, *42*, 1675–1680.

Anderson, L. A., and J. L. Sarmiento (1994), Redfield ratios of remineralization determined by nutrient data analysis, *Global Biogeochem. Cycles*, *8*, 65–80.

Antonov, J. I., S. Levitus, T. P. Boyer, M. E. Conkright, T. D. O'Brien, and C. Stephens (1998), *World Ocean Atlas 1998*, vol. 2, *Temperature of the Pacific Ocean*, *NOAA Atlas NESDIS 28*, NOAA, Silver Spring, Md.

Battle, M., M. Bender, M. B. Hendricks, D. T. Ho, R. Mika, G. McKinley, S.-M. Fan, T. Blaine, and R. F. Keeling (2003), Measurements and models of the atmospheric Ar/N_2 ratio, *Geophys. Res. Lett.*, *30*(15), 1786, doi:10.1029/2003GL017411.

Battle, M., et al. (2006), Atmospheric potential oxygen: New observations and their implications for some atmospheric and oceanic models, *Global Biogeochem. Cycles*, *20*, GB1010, doi:10.1029/2005GB002534.

Bender, M., T. Ellis, P. Tans, R. Francey, and D. Lowe (1996), Variability in the O_2/N_2 ratio of Southern Hemisphere air: Implications for the carbon cycle, *Global Biogeochem. Cycles*, *10*, 9–21.

Bishop, J. K. B., and W. B. Rossow (1991), Spatial and temporal variability of global surface solar irradiance, *J. Geophys. Res.*, *96*, 16,839–16,858.

Blackmon, M., et al. (2001), The Community Climate System Model, *Bull. Am. Meteorol. Soc.*, *82*, 2357–2376.

Böning, C. W., W. R. Holland, F. O. Bryan, G. Danabasoglu, and J. C. McWilliams (1995), An overlooked problem in model simulations of the thermohaline circulation and heat transport in the Atlantic Ocean, *J. Clim.*, *8*, 515–523.

Boyd, P. W., and E. R. Abraham (2001), Iron-mediated changes in phytoplankton photosynthetic competence during SOIREE, *Deep Sea Res., Part II*, *48*, 2529–2550.

Bryan, K. (1969), A numerical method for the study of the circulation of the world ocean, *J. Comput. Phys.*, *4*, 347–376.

Bryan, K. (1984), Accelerating the convergence to equilibrium of ocean-climate models, *J. Phys. Oceanogr.*, *14*, 666–673.

Capone, D. G., J. A. Burns, J. P. Montoya, A. Subramaniam, C. Mahaffey, T. Gunderson, A. F. Michaels, and E. J. Carpenter (2005), Nitrogen fixation by Trichodesmium spp.: An important source of new nitrogen to the tropical and subtropical North Atlantic Ocean, *Global Biogeochem. Cycles*, *19*, GB2024, doi:10.1029/2004GB002331.

Chavez, F., and J. R. Toggweiler (1995), Physical estimates of global new production: The upwelling contribution, in *Upwelling in the Ocean: Modern Processes and Ancient Records*, edited by C. P. Summerhayes et al., pp. 313–320, John Wiley, Hoboken, N. J.

Conkright, M. E., S. Levitus, and T. P. Boyer (1994), *World Ocean Atlas 1994*, vol. 1, *Nutrients*, *NOAA Atlas NESDIS 1*, 162 pp., NOAA, Silver Spring, Md..

Conkright, M. E., H. E. Garcia, T.D. O'Brien, R. A. Locarnini, T. P. Boyer, C. Stephens, and J. I. Antonov (2002), *World Ocean Atlas 2001*, vol. 4, *Nutrients*, *NOAA Atlas NESDIS 52*, edited by S. Levitus, 392 pp., NOAA, Silver Spring, Md.

Cox, M. D. (1984), A primitive equation, 3-dimensional model of the ocean, *GFDL Ocean Group Tech. Rep. 1*, 143 pp., Geophys. Fluid Dyn. Lab., Princeton, N. J.

Deutsch, C., S. Emerson, and L. Thompson (2005), Fingerprints of climate change in North Pacific oxygen, *Geophys. Res. Lett.*, *32*, L16604, doi:10.1029/2005GL023190.

Dietze, H., and A. Oschlies (2005), On the correlation between air-sea heat flux and abiotically induced oxygen gas exchange in a circulation model of the North Atlantic, *J. Geophys. Res.*, *110*, C09016, doi:10.1029/2004JC002453.

Doney, S. C., D. M. Glover, and R. G. Najjar (1996), A new coupled, one-dimensional biological-physical model for the upper ocean: Applications to the JGOFS Bermuda Atlantic Time-series Study (BATS) site, *Deep Sea Res., Part II*, *43*, 591–624.

Doney, S. C., W. G. Large, and F. O. Bryan (1998), Surface ocean fluxes and water-mass transformation rates in the coupled NCAR Climate System Model, *J. Clim.*, *11*, 1420–1441.

Dunne, J. P., R. A. Armstrong, A. Gnanadesikan, and J. L. Sarmiento (2005), Empirical and mechanistic models for the particle export ratio, *Global Biogeochem. Cycles*, *19*, GB4026, doi:10.1029/2004GB002390.

Emerson, S. (1987), Seasonal oxygen cycles and biological new production in surface waters of the subarctic Pacific Ocean, *J. Geophys. Res.*, *92*, 6535–6544.

Eppley, R. W., and B. J. Peterson (1979), Particulate organic matter flux and planktonic new production in the deep ocean, *Nature*, *282*, 677–680.

Falkowski, P. G., D. Ziemann, Z. Kolber, and P. K. Bienfang (1991), Role of eddy pumping in enhancing primary production in the ocean, *Nature*, *352*, 55–58.

Fasham, M. J. R. (1995), Variations in the seasonal cycle of biological production in sub-arctic oceans: A model sensitivity analysis, *Deep Sea Res., Part I*, *42*, 1111–1149.

Feely, R. A., C. L. Sabine, R. Schlitzer, J. L. Bullister, S. Mecking, and D. Greeley (2004), Oxygen utilization and organic carbon remineralization in the upper water column of the Pacific Ocean, *J. Oceanogr.*, *60*, 45–52.

Foujols, M.-A., M. Levy, O. Aumont, and G. Madec (2000), OPA 8.1 tracer model reference manual, 39 pp., Inst. Pierre Simon Laplace, Paris.

Ganachaud, A., and C. Wunsch (2002), Oceanic nutrient and oxygen transports and bounds on export production during the World Ocean Circulation Experiment, *Global Biogeochem. Cycles*, *16*(4), 1057, doi:10.1029/2000GB001333.

Garcia, H. E., and L. I. Gordon (1992), Oxygen solubility in sea water—Better fitting equations, *Limnol. Oceanogr.*, *37*, 1307–1312.

Garcia, H. E., and R. F. Keeling (2001), On the global oxygen anomaly and air-sea flux, *J. Geophys. Res.*, *106*, 31,155–31,166.

Geider, R. J., H. L. MacIntyre, and T. M. Kana (1997), A dynamic model of phytoplankton growth and acclimation: Responses of the balanced growth rate and the chlorophyll a:carbon ratio to light, nutrient-limitation and temperature, *Mar. Ecol. Prog. Ser.*, *148*, 187–200.

Gent, P. R., and J. C. McWilliams (1990), Isopycnal mixing in ocean circulation models, *J. Phys. Oceanogr.*, *20*, 150–155.

Gnanadesikan, A., R. D. Slater, N. Gruber, and J. L. Sarmiento (2002), Oceanic vertical exchange and new production: A comparison between models and observations, *Deep Sea Res., Part II*, *49*, 363–401.

Gnanadesikan, A., J. P. Dunne, R. M. Key, K. Matsumoto, J. L. Sarmiento, R. D. Slater, and P. S. Swathi (2004), Oceanic ventilation and biogeochemical cycling: Understanding the physical mechanisms that produce realistic distributions of tracers and productivity, *Global Biogeochem. Cycles*, *18*, GB4010, doi:10.1029/2003GB002097.

Gregg, W. W. (2002), Tracking the SeaWiFS record with a coupled physical/biogeochemical/radiative model of the global oceans, *Deep Sea Res., Part II*, *49*, 81–105.

Gruber, N., E. Gloor, S.-M. Fan, and J. L. Sarmiento (2001), Air-sea flux of oxygen estimated from bulk data: Implications for the marine and atmospheric oxygen cycles, *Global Biogeochem. Cycles*, *15*, 783–803.

Hamme, R. C., and S. R. Emerson (2006), Constraining bubble dynamics and mixing with dissolved gases: Implications for productivity measurements by oxygen mass balance, *J. Mar. Res.*, *64*, 73–95.

Hansell, D. A. (2002), DOC in the global ocean carbon cycle, in *Biogeochemistry of Marine Dissolved Organic Matter*, edited by D. A. Hansell and C. A. Carlson, pp. 685–715, Elsevier, New York.

Hansell, D. A., and C. A. Carlson (1998), Net community production of dissolved organic carbon, *Global Biogeochem. Cycles*, *12*, 443–453.

Jenkins, W. J., and J. C. Goldman (1985), Seasonal oxygen cycling and primary production in the Sargasso Sea, *J. Mar. Res.*, *43*, 465–491.

Josey, S. A., E. C. Kent, and P. K. Taylor (1998), The Southampton Oceanography Centre (SOC) ocean-atmosphere heat, momentum and freshwater flux atlas, *Rep. 6*, 30 pp., Southampton Oceanogr. Cent., Southampton, U. K.

Keeling, R. F., and S. R. Shertz (1992), Seasonal and interannual variations in atmospheric oxygen and implications for the global carbon cycle, *Nature*, *358*, 723–727.

Keeling, R. F., R. G. Najjar, M. L. Bender, and P. P. Tans (1993), What atmospheric oxygen measurements can tell us about the global carbon cycle, *Global Biogeochem. Cycles*, *7*, 37–67.

Keeling, R. F., B. B. Stephens, R. G. Najjar, S. C. Doney, D. Archer, and M. Heimann (1998), Seasonal variations in the atmospheric O_2/N_2 ratio in relation to the kinetics of air-sea gas exchange, *Global Biogeochem. Cycles*, *12*, 141–164.

Kolber, Z. S., R. T. Barber, K. H. Coale, S. E. Fitzwater, R. M. Greene, K. S. Johnson, S. Lindley, and P. G. Falkowski (2002), Iron limitation of phytoplankton photosynthesis in the equatorial Pacific Ocean, *Nature*, *371*, 145–149.

Large, W. G., J. C. McWilliams, and S. C. Doney (1994), Ocean vertical mixing: A review and a model with a nonlocal boundary layer parameterization, *Rev. Geophys.*, *32*, 363–403.

Large, W. G., G. Danabasoglu, S. C. Doney, and J. C. McWilliams (1997), Sensitivity to surface forcing and boundary layer mixing in a global ocean model: Annual-mean climatology, *J. Phys. Oceanogr.*, *27*, 2418–2447.

Laws, E. A., P. G. Falkowski, W. O. Smith, H. Ducklow, and J. J. McCarthy (2000), Temperature effects on export production in the open ocean, *Global Biogeochem. Cycles*, *14*, 1231–1246.

Lee, K. (2001), Global net community production estimated from the annual cycle of surface water total dissolved inorganic carbon, *Limnol. Oceanogr.*, *46*, 1287–1297.

LeQuéré, C., et al. (2005), Ecosystem dynamics based on plankton functional types for global ocean biogeochemistry models, *Global Change Biol.*, *11*, 2016–2040.

Levitus, S. (1982), Climatological atlas of the world ocean, *NOAA Prof. Pap. 13*, 173 pp., NOAA, Silver Spring, Md.

Libes, S. M. (1992), *An Introduction to Marine Biogeochemistry*, 745 pp., John Wiley, Hoboken, N. J.

Louanchi, F., and R. G. Najjar (2000), A global monthly climatology of phosphate, nitrate, and silicate in the upper ocean: Spring-summer export production and shallow remineralization, *Global Biogeochem. Cycles*, *14*, 957–977.

McGillicuddy, D. J., Jr., A. R. Robinson, D. A. Siegel, H. W. Jannasch, R. Johnson, T. D. Dickey, J. McNeil, A. F. Michaels, and A. H. Knap (1998), Influence of mesoscale eddies on new production in the Sargasso Sea, *Nature*, *394*, 263–265.

Moore, J. K., S. C. Doney, and K. Lindsay (2004), Upper ocean ecosystem dynamics and iron cycling in a global three-dimensional model, *Global Biogeochem. Cycles*, *18*, GB4028, doi:10.1029/2004GB002220.

Morel, A. (1988), Optical modeling of the upper ocean in relation to its biogenous matter content (case I waters), *J. Geophys. Res.*, *93*, 10,749–10,768.

Najjar, R. G., and R. F. Keeling (1997), Analysis of the mean annual cycle of the dissolved oxygen anomaly in the world ocean, *J. Mar. Res.*, *55*, 117–151.

Najjar, R. G., and R. F. Keeling (2000), Mean annual cycle of the air-sea oxygen flux: A global view, *Global Biogeochem. Cycles*, *14*, 573–584.

NCAR Oceanography Section (1996), The NCAR CSM Ocean Model, *Tech. Note NCAR/TN-423 + STR*, 84 pp., NCAR, Boulder, Colo.

Nevison, C. D., R. F. Keeling, R. F. Weiss, B. N. Popp, X. Jin, P. F. Fraser, L. W. Porter, and P. G. Hess (2005), Southern Ocean ventilation inferred from seasonal cycles of atmospheric N_2O and O_2/N_2 at Cape Grim, Tasmania, *Tellus, Ser. B*, *57*, 218–229.

Olson, R. J. (1981), Differential photoinhibition of marine nitrifying bacteria: A possible mechanism for the formation of the primary nitrite maximum, *J. Mar. Res.*, *39*, 227–238.

O'Neill, R. V., D. L. Angelis, J. J. Pastor, B. J. Jackson, and W. M. Post (1989), Multiple nutrient limitation in ecological models, *Ecol. Modell.*, *46*, 147–163.

Oschlies, A., W. Koeve, and V. Garçon (2000), An eddy-permitting coupled physical-biological model of the North Atlantic: 2. Ecosystem dynamics and comparison with satellite and JGOFS local studies data, *Global Biogeochem. Cycles*, *14*, 499–523.

Pacanowski, R. C., K. Dixon, and A. Rosati (1991), The GFDL modular ocean model users guide, *GFDL Ocean Group Tech. Rep. 2*, Geophys. Fluid Dyn. Lab., Princeton, N. J.

Sarmiento, J. L., R. D. Slater, and M. J. R. Fasham (1993), A seasonal three-dimensional ecosystem model of nitrogen cycling in the North Atlantic euphotic zone, *Global Biogeochem. Cycles*, *7*, 417–450.

Shea, D. J., K. E. Trenberth, and R. W. Reynolds (1990), A global monthly sea surface temperature climatology, *NCAR Tech. Note NCAR/TN-345*, 167 pp., NCAR, Boulder, Colo.

Shulenberger, E., and J. L. Reid (1981), The Pacific shallow oxygen maximum, deep chlorophyll maximum, and primary productivity, reconsidered, *Deep Sea Res., Part A*, *28*, 901–919.

Siegel, D. A., S. C. Doney, and J. A. Yoder (2002), The North Atlantic spring phytoplankton bloom and Sverdrup's critical depth hypothesis, *Science*, *296*, 730–733.

Spitzer, W. S., and W. J. Jenkins (1989), Rates of vertical mixing, gas exchange and new production: Estimates from seasonal gas cycles in the upper ocean near Bermuda, *J. Mar. Res.*, *47*, 169–196.

Wanninkhof, R. (1992), Relationship between wind speed and gas exchange over the ocean, *J. Geophys. Res.*, *97*, 7373–7382.

S. C. Doney, Department of Marine Chemistry and Geochemistry, Woods Hole Oceanographic Institution, Woods Hole, MA 02543, USA.

X. Jin, Institute of Geophysics and Planetary Physics and Department of Atmospheric and Oceanic Sciences, University of California, Los Angeles, CA 90095, USA.

F. Louanchi, Institut des Sciences de la Mer et de l'Aménagement du Littoral, Campus universitaire Dély Brahim, BP 19 Bois des Cars, Dely Brahim, 16320 Algiers, Algeria.

R. G. Najjar, Department of Meteorology, Pennsylvania State University, 503 Walker Building, University Park, PA 16802 USA. (najjar@meteo.psu.edu)